ICDT 2017

The Twelfth International Conference on Digital Telecommunications

April 23 - 27, 2017

Venice, Italy

ICDT 2017 Editors

Constantin Paleologu, University Politehnica of Bucharest, Romania
Stan McClellan, Texas State University - San Marcos, USA

ICDT 2017

Forward

The Twelfth International Conference on Digital Telecommunications (ICDT 2017), held between April 23-27, 2017 in Venice, Italy, continued a series of special events focusing on telecommunications aspects in multimedia environments. The scope of the conference was to focus on the lower layers of systems interaction and identify the technical challenges and the most recent achievements.

High quality software is not an accident; it is constructed via a systematic plan that demands familiarity with analytical techniques, architectural design methodologies, implementation polices, and testing techniques. Software architecture plays an important role in the development of today's complex software systems. Furthermore, our ability to model and reason about the architectural properties of a system built from existing components is of great concern to modern system developers.

Performance, scalability and suitability to specific domains raise the challenging efforts for gathering special requirements, capture temporal constraints, and implement service-oriented requirements. The complexity of the systems requires an early stage adoption of advanced paradigms for adaptive and self-adaptive features.

Online monitoring applications, in which continuous queries operate in near real-time over rapid and unbounded "streams" of data such as telephone call records, sensor readings, web usage logs, network packet traces, are fundamentally different from traditional data management. The difference is induced by the fact that in applications such as network monitoring, telecommunications data management, manufacturing, sensor networks, and others, data takes the form of continuous data streams rather than finite stored data sets. As a result, clients require long-running continuous queries as opposed to one-time queries. These requirements lead to reconsider data management and processing of complex and numerous continuous queries over data streams, as current database systems and data processing methods are not suitable.

The conference had the following tracks:
- Digital communications
- SMARTSYS: Issues in Smart Systems: Grids, Homes, Vehicles, Cities and the Internet of Things

We take here the opportunity to warmly thank all the members of the ICDT 2017 technical program committee, as well as all the reviewers. The creation of such a high quality conference program would not have been possible without their involvement. We also kindly thank all the authors that dedicated much of their time and effort to contribute to ICDT 2017. We truly believe that, thanks to all these efforts, the final conference program consisted of top quality contributions.

We also gratefully thank the members of the ICDT 2017 organizing committee for their help in handling the logistics and for their work that made this professional meeting a success.

We hope that ICDT 2017 was a successful international forum for the exchange of ideas and results between academia and industry and to promote further progress in the area of digital communications. We also hope that Venice, Italy provided a pleasant environment during the conference and everyone saved some time to enjoy the unique charm of the city.

ICDT 2017 Committee

ICDT Steering Committee
Constantin Paleologu, University Politehnica of Bucharest, Romania
Jaime Lloret Mauri, Polytechnic University of Valencia, Spain
Ioannis Moscholios, University of Peloponnese - Tripolis, Greece
Sathiamoorthy Manoharan, University of Auckland, New Zealand
Bernd E. Wolfinger, University of Hamburg, Germany

ICDT Industry/Research Advisory Committee
Tomohiko Taniguchi, Fujitsu Laboratories Limited, Japan
Scott Trent, IBM Research – Tokyo, Japan

ICDT 2017
Committee

ICDT Steering Committee

Constantin Paleologu, University Politehnica of Bucharest, Romania
Jaime Lloret Mauri, Polytechnic University of Valencia, Spain
Ioannis Moscholios, University of Peloponnese - Tripolis, Greece
Sathiamoorthy Manoharan, University of Auckland, New Zealand
Bernd E. Wolfinger, University of Hamburg, Germany

ICDT Industry/Research Advisory Committee

Tomohiko Taniguchi, Fujitsu Laboratories Limited, Japan
Scott Trent, IBM Research – Tokyo, Japan

ICDT 2017 Technical Program Committee

Akbar Sheikh Akbari, Leeds Beckett University, UK
Atallah Mahmoud AL-Shatnawi, Al al-Byte University, Jordan
Maria Teresa Andrade, FEUP / INESC Porto, Portugal
Mario Arrigoni Neri, Università di Bergamo, Italy
Ilija Basicevic, University of Novi Sad, Serbia
Andrzej Borys, Gdynia Maritime University, Poland
Fernando Cerdan, Universidad Politecnica de Cartagena, Spain
Paskorn Champrasert, Chiang Mai University, Thailand
Eleonora D'Andrea, University of Pisa, Italy
Wanyang Dai, Nanjing University, China
Abhishek Das, All India Council for Technical Education, Kolkata, India
Alexander Dudin, Belarusian State University, Belarus
Jingyuan Fan, University of New York at Buffalo, USA
Mahmood Fathy, Iran University of Science and Technology, Iran
Mário F. S. Ferreira, University of Aveiro, Portugal
Rita Francese, Università di Salerno, Italy
Francois Gagnon, Cégep Sainte-Foy, Canada
Katja Gilly, Universidad Miguel Hernández, Spain
Félix J. García Clemente, Universidad de Murcia, Spain
Andre Leon S. Gradvohl, University of Campinas, Brazil
Carlos Guerrero, University of Balearic Islands, Spain
Ahmad Yusairi Bani Hashim, Universiti Teknikal Malaysia Melaka, Malaysia
Daniela Hossu, University Politehnica of Buchatest, Romania
Yasin Kabalci, Nigde University, Turkey

Rob van der Mei, CWI and VU University Amsterdam, Netherlands
Antonio Virdis, University of Pisa, Italy
Sergei Volvenko, Peter the Great Saint-Petersburg Polytechnic University, Russia
Bernd E. Wolfinger, University of Hamburg, Germany
Ouri Wolfson, University of Illinois, USA
Wai Lok Woo, Newcastle University, UK
Ligang Zhang, Centre for Intelligent Systems, Central Queensland University, Brisbane, Australia
Piotr Zwierzykowski, Poznan University of Technology, Poland

Copyright Information

For your reference, this is the text governing the copyright release for material published by IARIA.

The copyright release is a transfer of publication rights, which allows IARIA and its partners to drive the dissemination of the published material. This allows IARIA to give articles increased visibility via distribution, inclusion in libraries, and arrangements for submission to indexes.

I, the undersigned, declare that the article is original, and that I represent the authors of this article in the copyright release matters. If this work has been done as work-for-hire, I have obtained all necessary clearances to execute a copyright release. I hereby irrevocably transfer exclusive copyright for this material to IARIA. I give IARIA permission or reproduce the work in any media format such as, but not limited to, print, digital, or electronic. I give IARIA permission to distribute the materials without restriction to any institutions or individuals. I give IARIA permission to submit the work for inclusion in article repositories as IARIA sees fit.

I, the undersigned, declare that to the best of my knowledge, the article is does not contain libelous or otherwise unlawful contents or invading the right of privacy or infringing on a proprietary right.

Following the copyright release, any circulated version of the article must bear the copyright notice and any header and footer information that IARIA applies to the published article.

IARIA grants royalty-free permission to the authors to disseminate the work, under the above provisions, for any academic, commercial, or industrial use. IARIA grants royalty-free permission to any individuals or institutions to make the article available electronically, online, or in print.

IARIA acknowledges that rights to any algorithm, process, procedure, apparatus, or articles of manufacture remain with the authors and their employers.

I, the undersigned, understand that IARIA will not be liable, in contract, tort (including, without limitation, negligence), pre-contract or other representations (other than fraudulent misrepresentations) or otherwise in connection with the publication of my work.

Exception to the above is made for work-for-hire performed while employed by the government. In that case, copyright to the material remains with the said government. The rightful owners (authors and government entity) grant unlimited and unrestricted permission to IARIA, IARIA's contractors, and IARIA's partners to further distribute the work.

Table of Contents

Optimisation of Heterogeneous Migration Paths to High Bandwidth Home Connections

Frank Phillipson

The Netherlands Organisation for Applied Scientific Research (TNO),
P.O.Box 96800, 2509 JE The Hague, The Netherlands
Email: {frank.phillipson}@tno.nl

Abstract—Operators are building architectures and systems for delivering voice, audio, and data services at the required speed for now and in the future. For fixed access networks, this means in many countries a shift from copper based to fibre based access networks. This paper proposes a method to optimise the migration path, heterogeneously per central office area, using geometric models as input. The method results in a detailed migration path that meets a required bandwidth coverage. For this, two models are presented. The first minimises the total costs meeting a bandwidth requirement per period, the second minimises the deviation from this bandwidth requirement meeting a budget constraint per period. While the data used for the migration path optimisation is in practice hard to gather, the use of geometric modelling is proposed. This modelling approach can estimate the total CapEx of a migration step using only two simple parameters per Central Office area.

Index Terms—Access networks; Migration Optimisation; Geometric Models

I. Introduction

Broadband internet is becoming a common utility service. Using connected electronic devices in and outside our homes, we use more and more data and demand connectivity 24/7. The used services are asking more bandwidth due to the integration of video into numerous services. Most of the home connections, access networks and systems, of telecom operators are not prepared to offer this, where incumbent operators mostly use copper telecommunication networks offering ADSL (Asymmetric Digital Subscriber Line) or VDSL (Very High Bitrate Digital Subscriber Line) techniques as service. Digital subscriber line (DSL) is a family of technologies, used to transmit digital data over copper lines. The operators have to make the costly step to Fibre to the Cabinet (FttCab), Fibre to the Curb (FttCurb) or, even more costly, the full step to Fibre to the Home (FttH), Fibre near the home (FntH) or Fibre to the Air (FttA). An example of FntH and FttA is a wireless home connection or a Hybrid fibre-wireless (FiWi) access network, where fibre is brought to a location near the homes, e.g., street lights [1], and the remaining distance is covered by WiFi or WiMax [2] [3]. However, the roll out of all these fibre connections will be taking in many countries too long to compete with the cable TV operators, active in those countries, who can offer the required bandwidth using DOCSIS, Data Over Cable Service Interface Specification. on

their Hybrid Fibre Coaxial (HFC) networks at this moment. This urges the operators to take intermediate steps, such as FttCurb, and to think about the optimal migration strategy.

The incumbent telecom operators can choose between various topology types to offer. In this paper, the term 'topology' is used for the way the physical fibres and equipment are designed. It comprises the question where to deploy fibres, where to deploy copper, where is the active or passive equipment placed. Each topology can run multiple technologies. For example, in the 'Full Copper' topology the operator offers the services from the Central Office. The operator still can choose to offer ADSL or VDSL (containing here all VDSL based technologies such as VDSL, VDSL2, Vectored VDSL2, Vplus etcetera) technology for this service. In this paper, four topology types are distinguished (see Fig. 1):

1) Full Copper: services are offered from the Central Office (CO) over a copper (twisted pair) cable, using DSL techniques.
2) Fibre to the Cabinet (FttCab): the fibre connection is extended to the cabinet. From the cabinet the services are offered over the copper cable, using DSL or G.Fast techniques.
3) Hybrid Fibre to the Home (Hybrid FttH): services are offered from a Hybrid FttH Node, which is connected by fibre, close to the customer premises, in the street or in the building. Here again VDSL and G.Fast techniques can be offered.
4) Full Fibre to the Home (Full FttH): the fibre connection is brought up to the customer premises.

If the operator starts with a Full Copper topology in a certain area, he has to decide on the next step: bringing the fibre connection all the way to the customers or use an intermediate step, where he brings the fibre closer to the customer, e.g., FttCab. Note that the operator can have a heterogeneous network, where in different areas a different topology is deployed and a different starting position for migration is found. To make in a certain area the decision mentioned before, the operator has to look at the pros and cons of all the options. For example, the deployment of FttCab can be much faster than Full FttH, as it requires less digging, the last part of the connection from the street to the access
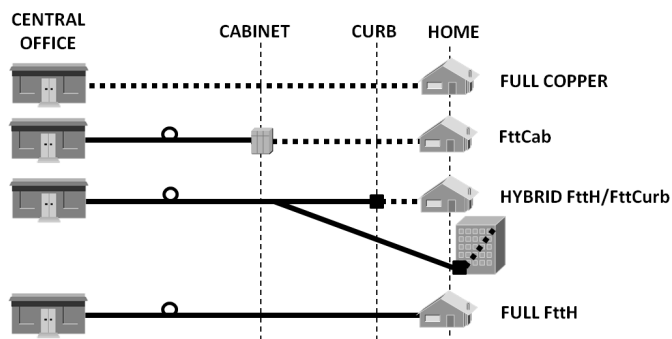
Figure 1. Four topologies.

node in the house does not have to be installed, and it meets the growing bandwidth demand for now and the near future. If, in future, this demand exceeds the supplied bandwidth, the remaining part to the residence can be connected with Full Fibre or using Hybrid Fibre as extra intermediate step. If the demand does not exceed the supplied bandwidth, for example it reaches some level of saturation, no further migration is needed, saving a lot of investments. However, when Full FttH is the expected final solution, using intermediate steps would incur investment and installation costs that might be lost and not reused.

This decision can be made on strategic level, for a bigger region or a whole country, or more tactical/operational within a region. In this paper, the option that the operator can decide per Central Office area which topology or technology to offer is regarded. This means that the operator is offering broadband as a service, instead of offering for example FttH as a service. If an operator decides on the topology or technique per Central Office area and per period (e.g., year), he can develop a detailed migration path that meets, for example, a bandwidth coverage in a larger area. This option is called a heterogeneous optimal migration path in contrast to a homogeneous optimal migration path, where one migration path is used for all Central Office areas within the bigger region. This is the first part where the novelty of this paper is in. Up to now, other papers only considered uniform migration paths or single migration paths.

The second part where this paper is novel, is the data used for the migration path optimisation. To estimate the costs of a topology and the migration from one topology to another topology, for each migration an optimal planning should be made. We propose to solve this by using the geometric modelling, as presented in [4] [5].

Concluding, in this paper, we present a methodology that can be used by operators to design their heterogeneous topology migration path from Full Copper to Full FttH, meeting their business requirements. First we start with a literature survey on related models. In Section III, a model is presented to optimise the heterogeneous migration paths. In Section IV, a method is presented to gather to input for the migration path optimisation using Geometric models. In Section V, the optimisation method is demonstrated by a case study. Finally, in Section VI, some conclusions are presented.

II. LITERATURE

Migration within telecommunication network is a topic in many Techno-Economical studies. In these studies the economic sanity of some choices are investigated. The European projects IST-TONIC [6] and CELTIC-ECOSYS [7] resulted in various upgrade or deployment scenarios for both fixed and wireless telecommunication networks, published in [8] and [9]. A major question in these studies is when to make the decision to roll out a FttC/VDSL network or a Full FttH network. Based on demand forecasts, it was shown that it is profitable to start in dense urban areas, wait for five years and then decide to expand it to the urban areas. With the use of real option valuation the effect of waiting is rewarded to identify the optimal decision over time. In [10] [11] the OASE approaches are presented for more in depth analysis of the FttH total cost of ownership (TCO) and for comparing different possible business models both qualitatively and quantitatively. The work of Casier [12] presents the techno-economic aspects of a fibre to the home network deployment. First he looks at all aspects of a semi-urban roll-out in terms of dimensioning and cost estimation models. Next, the effects of competition are introduced into the analysis. The work in [13] presents a multi-criteria model aimed at studying the evolution scenarios to deploy new supporting technologies in the access network to deliver broadband services to individuals and small enterprises. This model is based on a state transition diagram, whose nodes characterise a subscriber line in terms of service offerings and supporting technologies. This model was extended for studying the evolution towards broadband services and create the optimal path for broadband network migration. A similar kind of model is presented in [14] [15], where also an optimal strategy is proposed using a dynamic migration model. They study the best migration path including CAPEX, OPEX and revenues. Several fixed access technologies are taken as multiple intermediate steps. A more recent study [16] proposes several migration strategies for active optical networking from the data plane, topology, and control plane perspectives, and investigates their impact on the total cost of ownership but does not optimise.

Finally, our own previous work was about the benefits of a migration path as alternative for the direct step from Full Copper to FttH [17] and a Techno-Economic model [18] that can calculate the effect of offering different topologies and technologies in access networks (in migration) on market share, revenues, costs and earnings.

As said earlier, all these approaches (if optimising) only consider uniform or single migration paths and do not include the possibility of using geometric models as input.

III. MIGRATION MODEL

A migration path is defined here as a path from one topology/technique combination to a destination topol-
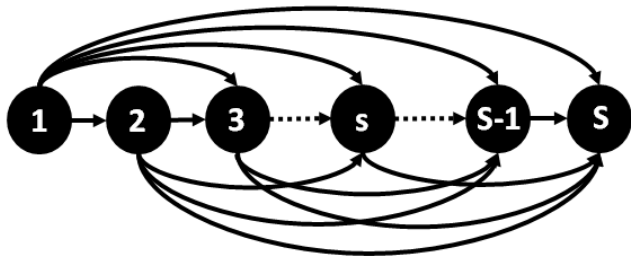
Figure 2. Migration paths.

TABLE II. DEFINITIONS

Notation		Description
i and j	=	indices for topologies/technology;
l	=	index for location, here CO area;
t	=	index for time period;
d	=	index for distance, e.g., 200, 400, 600 m;
y_{ilt}	=	1 if technology i active on time t, location l
x_{ijlt}	=	1 if migration from i to j in year t for location l;
c_{ijl}	=	migration costs going from i to j location l
o_{ilt}	=	OpEx technology i active on time t, location l
R_{ild}	=	Number houses reached by i within d meter for location l;
RT_l	=	Total number premises for location l;
G_{td}	=	Requested percentage of houses in total area, reached within d meter on time t;
B_t	=	Maximum budget in time t;

ogy/technique, possibly using other topology/technique combination as intermediate steps. Analogue to [14] we use a figure to clarify the idea, see Fig. 2. Each node here is a topology/technique combination. One can choose a path from node 1, typically Full Copper/ADSL, to node S, typically FttH. So examples for the paths are: Full Copper/ADSL to FttH, Full Copper/ADSL to FttCab/VDSL to FttH, Full Copper/ADSL to FttCab/VDSL to FttCurb/G.Fast, etcetera. The focus in this paper is on an area that consists of multiple Central Offices, which is the location of the switching equipment, to which subscriber home and business lines are connected on a local loop, for example a city or a district. The goal of the operator is to offer in this district a certain bandwidth coverage (per year), given a budget (per year) and possibly other constraints. A bandwidth coverage can be a single value, e.g., 'I want to offer 100 Mb/s in 2017', or a distribution over various bandwidth values in a number of years. An example of this distribution over years is presented in Table I. In the table is stated that in 2018 (at least) 60% of the houses need to have (at least) 100 Mb/s, at least 40% of the houses need to have (at least) 200 Mb/s and (at least) 10% need (at least) 300Mb. The percentages do not add up to 100% while they are exceedance probabilities. If all houses have a connection that offers 500 Mb/s the bandwidth coverage demand is met, obviously.

TABLE I. COVERAGE GOAL.

Year	100 Mb/s	200 Mb/s	300 Mb/s
2018	60%	40%	10%
2021	80%	60%	20%
2024	90%	80%	40%

Now, the problem can be defined as a mathematical Mixed Integer Programming Problem. The notation that is used is presented in Table II. First the objective function is defined as:

$$\min \sum_i \sum_j \sum_l \sum_t c_{ijl} x_{ijlt}. \quad (1)$$

This objective minimises the total costs for the migration and

needs to be met under the following constraints:

$$\sum_i \sum_j x_{ijlt} \le 1, \quad \forall t, l \quad (2)$$

$$\sum_i y_{ilt} = 1, \quad \forall l, t \quad (3)$$

$$x_{ijlt} \ge \frac{1}{2}(y_{jlt} - y_{jlt-1}) - \frac{1}{2}(y_{ilt} - y_{ilt-1}) - \frac{1}{2} \forall i, j, l, t \quad (4)$$

$$\frac{\sum_i \sum_l R_{ild} \cdot y_{ilt}}{\sum_l RT_l} \ge G_{td}, \quad \forall t, d \quad (5)$$

This model will be called the base model. In (1) the total investment cost (CapEx) is minimised. In (2) it is made certain that there is not more than 1 migration step per year per location. Equation (3) makes sure that each location has each year exactly 1 topology. Equation (4) creates the migration steps. The right term can only be greater than zero if (and only if) $(y_{jlt} - y_{jlt-1}) = 1$ and $(y_{ilt} - y_{ilt-1}) = -1$, which indicates that there is a transition from technology i to technology j. In (5) the demanded bandwidth coverage is required.

An alternative objective function is realised when adding the operational cost, or OpEx. This alters the objective function in:

$$\min \sum_i \sum_j \sum_l \sum_t c_{ijl} x_{ijlt} + \sum_i \sum_l \sum_t o_{ilt} y_{ilt} \quad (6)$$

An alternative model is the model in which there exists a budget constraint per time period. In this formulation the budget constraints are hard, where the gap between the realised and demanded bandwidth per year is minimised:

$$\min \sum_t \sum_d \left(G_{td} - \frac{\sum_i \sum_l R_{ild} \cdot y_{ilt}}{\sum_l RT_l} \right), \quad (7)$$

under the following constraints:

$$\sum_i \sum_j x_{ijlt} \leq 1, \quad \forall t, l \quad (8)$$

$$\sum_i y_{ilt} = 1, \quad \forall l, t \quad (9)$$

$$x_{ijlt} \geq \frac{1}{2}(y_{jlt} - y_{jlt-1}) - \frac{1}{2}(y_{ilt} - y_{ilt-1}) - \frac{1}{2}\forall i, j, l, t \quad (10)$$

$$\sum_i \sum_j \sum_l c_{ijl} x_{ijlt} \leq B_t, \quad \forall t \quad (11)$$

where (11) is added as budget constraint.

IV. INPUT FROM GEOMETRIC MODEL

In the previous section two parameters are used, that are not that easy to get, namely c_{ijl}, the cost for migration from i to j on location l, and R_{ild}, the number of premises reached by i within d meter on location l. To get the value of these parameters, for each migration an optimal planning should be made. We introduce an alternative for this problem by using the outcomes of geometric modelling, as presented in [4] [5]. This means that we start by a simple set of parameters per (currently) active node: the total cable length (D) and the capacity of this node (n), which equals the number of premises connected. As is shown in [5] from these parameters the geometric density of the premises can be derived. With this geometric density we can estimate the number of new active locations that a next technology needs in this area to achieve a certain distance coverage and, consequently, the bandwidth coverage. From this number of active elements the costs of the migration can be estimated. Next, using the same density also the cable and digging distances to connect those new active elements can be estimated.

To illustrate this approach, think of an area, currently equipped with VDSL2, that contains $n_1 = 1,000$ houses. The given total cable length equals $D_1 = 875,000$ meter. Now, the parameter d, which indicates the house density of the area, expressed in the (average) width of the premises, can be derived by solving (using $s_1 = \sqrt{n_1}$):

$$d = \frac{D_1}{2 \cdot s_1 \cdot \lceil \frac{1}{2}s_1 \rceil \cdot \lfloor \frac{1}{2}s_1 \rfloor}. \quad (12)$$

Resulting in $d_D = 57, 7$ for the given example. Let us assume that in the next topology, let us assume V-plus, we want to reach 85% within 400 meters. From [4] we know the probability distribution of the individual distances of the houses to the active node: it can be estimated by a Normal distribution $F_{\mu,\sigma}(x)$ with $\mu_2 = \frac{D_2}{n_2}$ and $\sigma_2 = \frac{M-\mu}{2}$ where M_2 represents the maximum cable distance in the second topology using [5]:

$$M = 2 \cdot \lceil \frac{1}{2}s_2 - 1 \rceil \cdot d + 0.5d, \quad (13)$$

$$s_2 = \sqrt{n_2}, \quad (14)$$

and the total cable length in the second topology

$$D_2 = 2 \cdot d \cdot s_2 \cdot \lceil \frac{1}{2}s_2 \rceil \cdot \lfloor \frac{1}{2}s_2 \rfloor. \quad (15)$$

Now, the question is to choose n_2 such that $F_{\mu(n_2),\sigma(n_2)}(300) = 0.90$. This can be solved numerically and leads to the following values $n_2 = 100$, $M_2 = 490$, $D_2 = 28800$, $\mu_2 = 290$ and $\sigma_2 = 100$. This means that to meet this requirement of 85% within 400 meter, 10 new nodes should be installed. It takes 28800 meter of digging and (fibre) cable to connect these nodes.

V. CASE STUDY

In this section a case study is presented introducing a small city with 40 cabinets and 18,500 houses. The current employment is ADSL. The operator has a bandwidth coverage goal, expressed in percentage of the houses that is within a certain distance from the active equipment. The coverage goal is shown in Table III. For example, the goal is to have 70% of the houses within 400 meter in 2021.

TABLE III. COVERAGE GOAL.

Year	600m	400m	200m
2018	70%	40%	20%
2021	85%	70%	30%
2024	85%	85%	40%

TABLE IV. PER PERIOD OPTIMISATION - BASE MODEL.

Year	ADSL	VDSL	V-plus
2018	23	7	10
2021	17	7	16
2024	5	7	28

TABLE V. OVERALL OPTIMISATION - BASE MODEL.

Year	ADSL	VDSL	V-plus
2018	25	0	15
2021	18	1	21
2024	8	6	26

Two cases are distinguished. In the first case the operator tries to meet the distance requirement for each year independently and optimally. This means that the operator optimises the design of each area without knowledge of future networks, topologies and technologies. In the second case the operator tries to meet the requirements for the total time horizon, using the methodology of Section III. For each cabinet, for each 3-year period, the operator can chose between doing nothing, implementing VDSL and implementing V-plus, each with its own costs and bandwidth consequences. Now, the operator tries to make the decisions such that the total migration costs are minimal, meeting the distance coverage requirements for each period as modelled in the base model of Section III. The used costs for digging and equipment are based on the (Sub-Urban) numbers of [19].

The result of the optimisation (only using Excel and OpenSolver [20]) of the two cases is depicted in Table IV for the per-period optimisation and Table V for the overall

optimisation. In the per-period optimisation in the first year (2018) more VDSL is chosen, as this is a cheaper solution to meet the 2018 requirements. In the overall optimisation the more expensive choice for V-plus is made, as this is more ready for the future. In the other two stages more or less the same choices are made. This leads to the total overview of costs as depicted in Fig. 3, where the total costs of the overall optimisation are lower, but the costs in the first year are higher. All costs are expressed in Net Present Value, with an average cost of capital of 6%, making the values in the various years comparable.
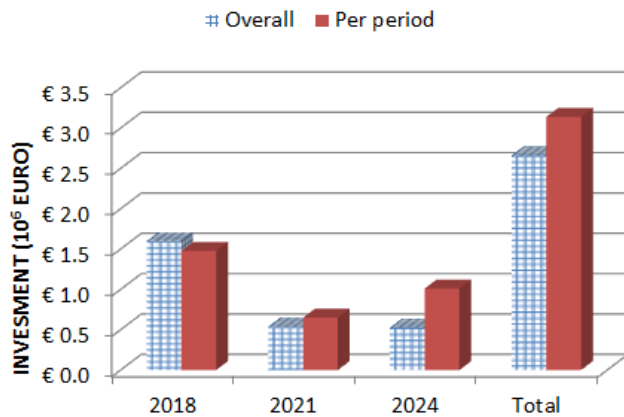
Figure 3. Investment costs.
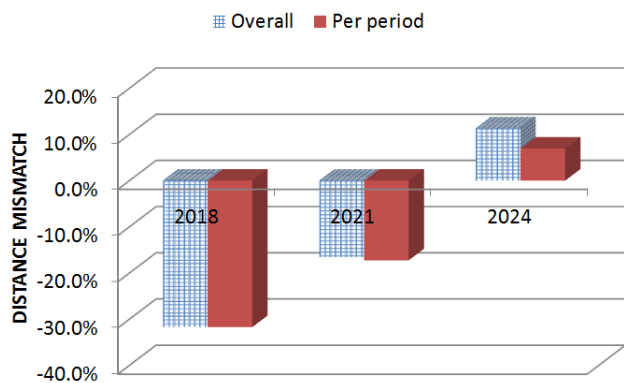
Figure 4. Meeting the bandwidth demand in the alternative model.

If the alternative model is used with a maximum budget of 750,000 euro per period, the results are as depicted in Fig. 4. In the first two year the bandwidth demand cannot be met, with a cumulative difference of 32% for the both approaches. This means that the sum of the differences between the number of houses reached within a certain distance and the requested percentage for all distances in a certain year equals 32%. In the second time period there also is almost no difference (0.7%), but in the third period, the small differences in the first two periods pay off, by a big difference in realisation (6.9% versus 11.3%). This means that the overall optimisation realised a plus on coverage of more than 4%.

TABLE VI. PER PERIOD OPTIMISATION - ALTERNATIVE MODEL.

Year	ADSL	VDSL	V-plus
2018	30	0	10
2021	13	2	15
2024	12	3	25

TABLE VII. OVERALL OPTIMISATION - ALTERNATIVE MODEL.

Year	ADSL	VDSL	V-plus
2018	31	0	9
2021	24	0	16
2024	10	4	26

The result of the optimisation of the two cases is depicted in Table VI for the per-period optimisation and Table VII for the overall optimisation. What can be seen in this example is that the alternative model over-compensates the under performance in the first two periods by over performance in the last period. This can be prevented by an other choice of objective in this model (Eq. 7), such as

$$\min \sum_t \sum_d \max\left(0, G_{td} - \frac{\sum_i \sum_l R_{ild} \cdot y_{ilt}}{\sum_l RT_l}\right) \quad (16)$$

or

$$\min \sum_t \sum_d \left(G_{td} - \frac{\sum_i \sum_l R_{ild} \cdot y_{ilt}}{\sum_l RT_l}\right)^2. \quad (17)$$

Equation 16 is the best in preventing this phenomenon, while compensating is not possible: the negative terms are set to zero. Equation 17 tries to get results close to zero, preventing big deviations. Both alternatives will result in a model that is harder to solve than before by introducing a non-linear objective.

VI. CONCLUSION

In this paper, we presented a methodology that can be used by operators to design their heterogeneous topology migration path from Full Copper to (Full) FttH, meeting their business requirements. Heterogeneous means that the operator decides per Central Office area the topology or technique per period (e.g., year), resulting in a detailed migration path that meets a required bandwidth coverage in the larger area. For this, two models were presented. The first minimised the total investment (CapEx) and operational costs (OpEx), such that the bandwidth requirement per period was met. The second minimised the deviation from this bandwidth requirement meeting a budget constraint per period.

The data used for the migration path optimisation is in practice hard to gather. For this, the use of geometric modelling was proposed, with which the total CapEx of a migration step can be estimated using only two parameters per Central Office area, the total existing cable length and the capacity of this node.

Finally, the two models were demonstrated in two case studies that showed the gain that can be realised by the migration path optimisation.

REFERENCES

[1] T. Vos, *Using Lampposts to Provide Urban Areas with Multiple Services*. MSc Thesis, Erasmus University Rotterdam and TNO, 2016.

[2] N. Ghazisaidi, M. Maier, and C. M. Assi, "Fiber-wireless (fiwi) access networks: A survey," *IEEE Communications Magazine*, vol. 47, no. 2, pp. 160–167, 2009.

[3] F. D'Andreagiovanni, F. Mett, and J. Pulaj, "Towards the integration of power-indexed formulations in multi-architecture connected facility location problems for the optimal design of hybrid fiber-wireless access networks," in *OASIcs-OpenAccess Series in Informatics*, vol. 50. Schloss Dagstuhl-Leibniz-Zentrum fuer Informatik, 2016, pp. 1–11.

[4] F. Phillipson, D. Worm, N. Neumann, A. Sangers, and S.-J. Wiarda, "Estimating bandwidth coverage using geometric models," in *Networks and Optical Communications (NOC), 2016 21st European Conference on*. IEEE, 2016, pp. 152–156.

[5] F. Phillipson, "Estimating ftth and fttcurb deployment costs using geometric models with enhanced parameters," in *Networks and Optical Communications-(NOC), 2015 20th European Conference on*. IEEE, 2015, pp. 1–5.

[6] IST-TONIC. Retrieved February 2017. [Online]. Available: cordis.europa.eu/result/rcn/81333_en.html

[7] CELTIC-ECOSYS. Retrieved February 2017. [Online]. Available: www.celticplus.eu/project-ecosys

[8] T. Rokkas, D. Katsianis, and D. Varoutas, "Techno-economic evaluation of FttC/VDSL and FttH roll-out scenarios: Discounted cash flows and real option valuation," *Journal of Optical Communications and Networking*, vol. 2, no. 9, pp. 760–771, 2010.

[9] T. Monath, N. Elnegaard, P. Cadro, D. Katsianis, and D. Varoutas, "Economics of fixed broadband access network strategies," *IEEE Communications Magazine*, vol. 41, no. 9, pp. 132–139, 2003.

[10] S. Verbrugge *et al.*, "Research approach towards the profitability of future FttH business models," in *Proceedings Telecommunications Network Strategy and Planning Symposium (NETWORKS)*, Warshaw, Poland, June 2011, pp. 1–10.

[11] M. Forzati *et al.*, "Next-generation optical access seamless evolution: Concluding results of the european fp7 project oase," *Journal of Optical Communications and Networking*, vol. 7, no. 2, pp. 109–123, 2015.

[12] K. Casier, *Techno-Economic Evaluation of a Next Generation Access Network Deployment in a Competitive Setting*. Universiteit Gent, 2009.

[13] C. Antunes, J. Craveirinha, and J. Clímaco, "Planning the evolution to broadband access networks: A multicriteria approach," *European Journal of Operational Research*, vol. 109, no. 2, pp. 530–540, 1998.

[14] R. Zhao, L. Zhou, and C. Mas Machuca, "Dynamic migration planning towards FttH," in *Telecommunications Network Strategy and Planning Symposium (NETWORKS)*, Warshaw, Poland, September 2010, pp. 1617–1622.

[15] R. R. Reyes, R. Zhao, and C. M. Machuca, "Advanced dynamic migration planning toward ftth," *IEEE Communications Magazine*, vol. 52, no. 1, pp. 77–83, 2014.

[16] K. Wang *et al.*, "Migration strategies for fttx solutions based on active optical networks," *IEEE Communications Magazine*, vol. 54, no. 2, pp. 78–85, 2016.

[17] F. Phillipson, "A cost effective topology migration path towards fibre," *Lecture Notes on Information Theory Vol*, vol. 2, no. 1, 2014.

[18] F. Phillipson, C. Smit-Rietveld, and P. Verhagen, "Fourth generation broadband delivered by hybrid ftth solutiona techno-economic study," *Journal of Optical Communications and Networking*, vol. 5, no. 11, pp. 1328–1342, 2013.

[19] T. Rokkas, "Techno-economic analysis of pon architectures for ftth deployments: Comparison between gpon, xgpon and ng-pon2 for a greenfield operator," in *Telecommunication, Media and Internet Techno-Economics (CTTE), 2015 Conference of*. IEEE, 2015, pp. 1–8.

[20] A. Mason, "Opensolver an open source add-in to solve linear and integer progammes in excel," in *Operations Research Proceedings 2011*, ser. Operations Research Proceedings, D. Klatte, H.-J. Lathi, and K. Schmedders, Eds. Springer Berlin Heidelberg, 2012, pp. 401–406.

A Low-Overhead Framework for Inexpensive Embedded Control Systems

Ivan Cibrario Bertolotti[*], Tingting Hu[§], and Gilda Ghafour Zadeh Kashani[*]

[*] National Research Council of Italy – IEIIT, Torino, Italy
Email: {ivan.cibrario, gilda.kashani}@ieiit.cnr.it
[§] University of Luxembourg – Faculty of Science, Technology and Communication, Luxembourg
Email: tingting.hu@uni.lu

Abstract—**Embedded control systems are becoming more and more popular, especially in relatively inexpensive consumer products, like home appliances and building automation controllers. As a consequence, there is an ever increasing desire to reduce firmware development time and cost, without hampering reliability and performance. In this paper, a low-overhead firmware development framework is proposed, which allows programmers to develop and deploy typical real-time control software faster than using plain C-language programming. At the same time, experimental results confirm the framework's efficiency and applicability even to low-end microcontrollers.**

Keywords–Embedded control systems; Logic controllers; Firmware development frameworks.

I. Introduction and Related Work

The ever-increasing popularity of inexpensive control systems—mainly driven by consumer products, which nowadays invariably include at least one embedded processor—brings new challenges to firmware development. This market segment is characterized by fierce competition that forces vendors to reduce costs and shrink time to market, a fact that strongly encourages the introduction of more abstraction in the development process.

This often entails the adoption of new programming techniques. For instance, [1] discusses a framework that works according to an event-driven paradigm and UML statecharts. Similarly, programming environments for Programmable Logic Controllers (PLCs) [2], either proprietary [3] or open-source [4], are indeed quite powerful. Nevertheless, they force programmers to learn dedicated languages they are unlikely familiar with, for instance, the ones defined in [5]. Moreover, the cost of a PLC is typically much higher than the cost of a microcontroller-based board of equivalent processing power. In the case of [6], the framework indeed adopts a simplified dialect of the C++ language. However, the programming model consists of a single main-loop that contains the code to be executed, and must be suitably extended to support real-time multitasking [7].

Staying with the easiest and probably most widespread embedded systems programming language—that is, the C language [8]—brings the additional advantage of making readily available a variety of sophisticated open-source firmware components, ranging from real-time operating systems (RTOS) [9] to filesystems [10] and TCP/IP protocol stacks [11]. Previous proposals, like the one described in [12], succeeded to leverage these components and speed up firmware development, but they still lack much needed abstraction. In the paper, a firmware development framework is proposed, whose goal
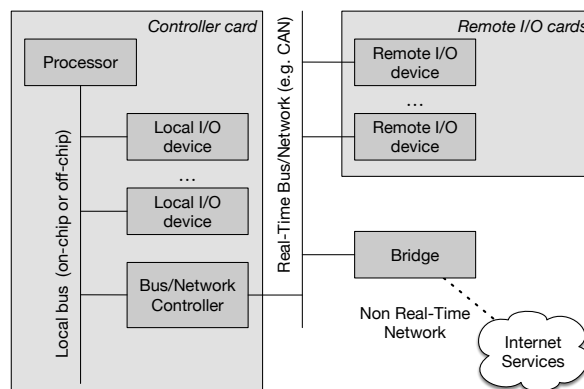
Figure 1. Hardware architecture of a typical distributed control system.

is to shield application-level firmware developers from most low-level architectural details and abstract from Input–Output (I/O) mechanisms through a flexible configuration system. At the same time, programmers may still use the C language, thus reaching a convenient trade-off between the two goals discussed previously.

Real-time execution models have been the subject of considerable debate since a long time [13]. Even though other, more sophisticated models have been proposed [14], the framework proposed in this paper sticks with a traditional *cyclic executive* [15] for the real-time control part to boost performance and reduce overheads. In order to overcome the inflexibility of the method when considered alone [13] [14], it has been blended with a more general task-based system, coordinated by the underlying FREERTOS RTOS. The paper is organized as follows. Section II describes how the framework has been designed and discusses its architecture. Next, Section III provides more information about its implementation, focusing on two critical aspects. Section IV presents the experimental evaluation, as well as the related measurement method, and Section V concludes the paper.

II. Framework Design and Architecture

A. Main Features and Design Guidelines

In recent years, a generalized trend in the design and implementation of embedded control systems has been to shift from a concentrated to a distributed I/O paradigm. Accordingly, as shown in Figure 1, the framework supports *local* I/O devices, reachable by the processor by means of an on-chip or off-chip
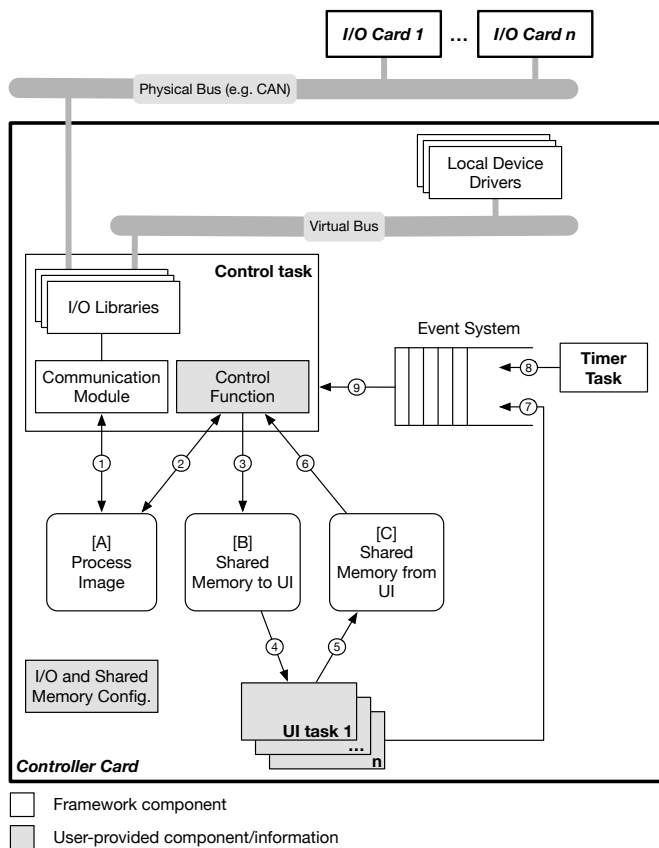
Figure 2. Simplified framework architecture.

bus local to the controller card, as well as *remote* I/O cards and devices, which are connected to the processor by means of a real-time communication network.

Furthermore, the framework enables firmware programmers to focus on the application-level part of design and development, such as the control algorithm. More specifically, it allows firmware programmers to operate on abstract *process image* (PI) variables, which represent the state of system inputs and outputs, regardless of how and where they are physically implemented. Last, but not least, even though some features of the framework resemble the ones provided by PLCs [2], in our case programmers shall be able to develop embedded control code using the C language [8] directly. Therefore, the above-mentioned PI variables are made available to programmers as any other, ordinary C-language variable is.

An additional feature of the framework, shown in the bottom-right part of Figure 1, is to provide access to the Internet through a bridge card. This feature is extremely important to implement key functionality, such as data logging, supervision, and firmware upgrades. However, it will not be further discussed in this paper for conciseness.

B. Framework Architecture

As it can be seen in Figure 2, the framework coordinates two groups of tasks that together form the complete control system and its user interface (UI). The first group of task consists of a *control* task, as well as a *timer* task. These two tasks implement the real-time control cycle, to be described in more details in Secton II-C. The only user-written code in

this group is an embedded *control function*, which executes the control algorithm cyclically when invoked by the framework. A memory area, denoted as [A] in the figure, holds the aforementioned PI variables and is accessible to control task components only. The second group of tasks is outside the scope of the framework. All tasks in this group are completely user-written—except for what concerns their interface to the first group—and they cooperate to realize the system UI. Communication and data sharing between the two groups take place by means of two shared memory areas, denoted as [B] and [C] in Figure 2, one for each transfer direction (to or from the UI tasks, respectively).

The same figure also depicts the main data flows internal to the control system and managed by the framework, identified by means of circled numbers. More specifically:

- The *communication module* and the control function, both within the control task, have read-write access to memory [A] through data flows ① and ②, respectively. The role of the control function has already been mentioned before. On the other hand, the communication module is responsible of updating PI variables cyclically. In order to transparently support multiple physical implementations of those variables, all I/O functions are mediated by appropriate I/O libraries. For instance, the current implementation supports Modbus CAN [16] I/O cards, as well as local I/O devices by means of device drivers.
- Data flows ③ through ⑥ implement communication with the UI tasks. Unlike memory [A], memories [B] and [C] are protected against concurrent access by means of mutual exclusion locks with definite time-outs on the real-time side. The decision of having two memory areas, each supporting a unidirectional data flow, is useful to reduce lock contention and improve granularity. At the same time, keeping memory [A] totally separate from [B] and [C] also works as a safeguard against unintentional or unauthorized access to PI variables by non real-time tasks. Data sharing among these areas is implemented in a controlled way by the framework, through the control task itself, by periodically mirroring a pre-configured subset of PI variables to/from [B] and [C].
- As it will be better discussed in Section II-C, the control task implements a traditional control cycle. On the other hand, UI tasks are event driven and, sporadically, may need to convey expedited information to the control task itself. This is done by generating and sending *sporadic events* to it, according to flow ⑦ of Figure 2. As a consequence, the control task has to react to two event sources: one *cyclic*, and one *sporadic*. Cyclic events are generated by the timer task and correspond to flow ⑧ in the figure. These two event sources are prioritized and combined into flow ⑨ by a dedicated *event system*, which also takes into account some peculiarities and shortcomings of the underlying RTOS. More details about event system implementation are given in Section III-B.

C. Control Cycle

Figure 3 contains a more detailed view of the control cycle implemented by the framework, along with sporadic events handling. Individual control cycles are triggered by
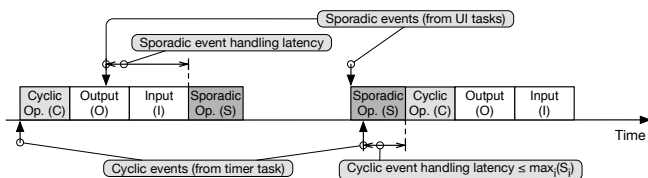
Figure 3. Control cycle and sporadic event handling.

```
BOARD_INSTANCE_LOCAL(
  sample_class, instance_name, 0,
  LOCAL_INPUT_VARIABLE(input_0,
    char, push_button, no_converter, NULL)
  LOCAL_OUTPUT_VARIABLE(output_0,
    char, led, no_converter, NULL))
```

Figure 4. Sample local I/O device configuration.

cyclic events generated by the timer task and consist of three phases. The *computation* phase (C phase) is implemented by the user-written control function. It operates on input PI variables collected in the previous cycle and computes output PI variables. It is followed by an *output* phase (O) that commits output PI variables and by an *input* phase (I), which collects input PI variables for the next cycle.

The same control function also handles sporadic events sent by UI tasks. Since the control task is single-threaded, two different kinds of interference are possible.

1) Any sporadic event generated while cyclic activities are in progress is postponed until the control task has completed them, as depicted in the left part of Figure 3.

2) Sporadic event handling (S) runs to completion after it starts. Therefore, as shown in the right part of the figure, if a cyclic event arrives while sporadic event handling is in progress, the start of the next cycle is delayed.

No provisions are made to bound the first kind of interference, since UI tasks are not considered hard real-time. On the other hand, the worst case for the second kind of interference is upper-bounded by the event system prioritization mechanism, which always delivers cyclic rather than sporadic events when both are available. As depicted in the right part of Figure 3, denoting with S_i the worst-case handling time for sporadic event i, the maximum interference is bounded by $\max_i(S_i)$, regardless of the number of pending sporadic events.

As an additional safeguard against dedicating excessive (high-priority) control task execution time to sporadic events, the event system implementation also prevents UI tasks from making more than a configurable number k of sporadic events pending. The implementation is based on a simple back pressure mechanism within the sporadic event generation primitive, better detailed in Section III-B.

D. Configuration Workflow

The last part of user-written code to be discussed in this paper and shown in the bottom-left corner of Figure 2, is the *I/O and shared memory configuration* files. The I/O configuration file contains a set of C macro invocations that define which local and remote I/O devices are configured in the system, as well as their relationship with PI variables. Quite intuitively, the shared memory configuration file plays a similar role concerning the structure of shared memories [B] and [C] and their relationship with PI variables, through the mirroring mechanism discussed in Section II-B.

As an example, Figure 4 shows how a simple local I/O device is configured. The device is called `instance_name` and belongs to device class `sample_class`. Class-related information is retrieved from a device database, not discussed here for conciseness. In this particular case, it is known from the database that devices belonging to `sample_class` implement a physical input `input_0` and a physical output `output_0`.

The I/O configuration file establishes that `input_0` is connected to a push button whose state will be accessible by means of PI variable `char push_button`, without any conversion. In fact, the configuration states to use the `no_converter` conversion function, with `NULL` parameter. The configuration contains similar information about the physical output, which is connected to a LED accessible through PI variable `char led`.

Using this approach, the control function works directly on `push_button` and `led`, using ordinary C-language statements, and the framework reflects their values to/from the corresponding physical I/O points in a completely transparent way. Thus, redesigning the system by moving an I/O point from a local device to a remote I/O board, for instance, becomes a matter of updating the I/O configuration file and does not require any changes to the control code. On the other hand, the firmware must be rebuilt, because configuration files are currently parsed at compile time and the framework does not support dynamic reconfiguration.

III. IMPLEMENTATION HIGHLIGHTS

This section complements Section II by highlighting two important implementation aspects and providing more details about them.

A. Input-Output Abstraction

One of the main framework design goals is the complete separation of the user-written control function from I/O-related details. Figure 5 outlines the multi-stage process that the framework implements to reach this goal. More specifically, the figure represents how the framework handles the `push_button` input PI variable, declared as shown in Figure 4. Output variables are handled in a similar way.

During the I phase of the control cycle (see Figure 3) the communication module scans the PI table, depicted at the bottom left of Figure 5. For each variable, the framework locates and invokes the appropriate device driver input method (which is responsible of retrieving the value of the variable from the device it resides on) and converter function (to convert the variable from its device-specific representation into a format suitable for the control function). This is done by following appropriate pointers rooted at the PI table.

As a result, in our example the current state of the push button is reflected into variable `char push_button`. The user-written control function can then use this variable during the C phase of the control cycle. No explicit synchronization mechanisms are needed because the I and C phases are executed sequentially within the control task. The framework
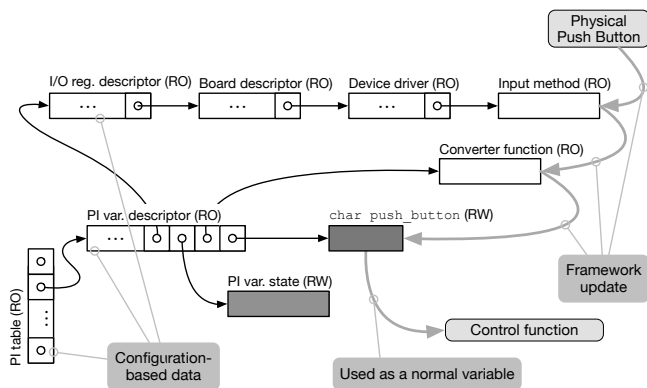
Figure 5. I/O abstraction process and related data structures.

Figure 6. Detailed view of event system implementation.

also associates and optionally makes available to the user additional per-variable state information, which summarizes the outcome of the operations just mentioned.

It is important to remark that the framework defines all data structures shown in Figure 5 automatically, starting from configuration items like the one shown in Figure 4. With the exception of PI variables themselves (like `push_button`) and their state information, all these data structures are completely hidden from the user. Furthermore, by means of a careful data structure design and layout, it was possible to share information as much as possible and store most data in read-only Flash memory.

As an example, board descriptions and device driver data structures are known to be immutable and are shared among all boards belonging to the same class. This is convenient to minimize memory consumption and, even more, save read-write memory that is often scarce in low-cost embedded systems. Referring back to Figure 5, the only read-write structures—to be stored in RAM—are the dark-gray-colored ones.

B. Event System

The event system consists of a FREERTOS message queue Q and a counting semaphore R. Figure 6 portrays a more detailed view of its implementation. For consistency, labels on event flows have been kept the same as in Figure 2. Instead, labels on semaphore primitives are enclosed in gray circles and summarize the primitive itself (P corresponds to *take* and V corresponds to *give*, when using FREERTOS's nomenclature).

The main event system design goal is to support generation and buffering of up to N events, of which $N-1$ are sporadic and one is cyclic. As remarked in Section II-C, in order to bound control cycle jitter due to interference with sporadic event handling, the cyclic event must be given higher priority than the others. This goal is accomplished by means of two distinct mechanisms:

1) Although FREERTOS does not implement fully prioritized message queues, it does provide a primitive to send a message to the *front* of a queue rather than the back. The event system makes use of this feature when sending a cyclic event to Q. Sporadic events are sent to the back, and hence, handled in a FIFO fashion.

2) By itself, prioritizing operations on Q is insufficient to grant cyclic events expedited handling, if Q is
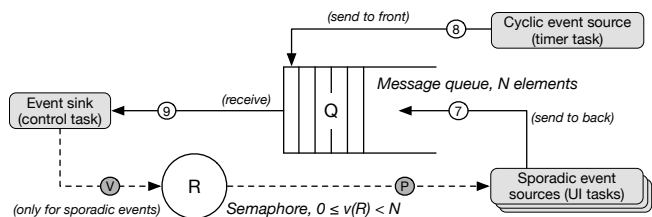
completely full when a cyclic event occurs. In this case any send operation—regardless of whether it is directed to the front or to the back—blocks the caller and FREERTOS does not offer any built-in mechanism to address this issue. Therefore, R is used as a rate control semaphore to bound the number of pending sporadic events to $N-1$, and hence, reserve one element of Q for cyclic events at any time.

To implement rate control, R is used according to the following protocol:

- the initial value of R is $N-1$;
- before sending a sporadic event to Q, the event system performs a P on R, blocking if necessary;
- after receiving a sporadic event from Q, the event system performs a V on R.

As a side effect, neglecting transients in between semaphore and queue operations, the current value of R, denoted as $v(R)$ in Figure 6, is always $0 \leq v(R) < N$ and represents how many elements of Q are available to sporadic events.

IV. EXPERIMENTAL EVALUATION

This part of the paper reports on the performance of the proposed framework and estimates its overhead. The experimental setup conforms to the architecture portrayed in Figure 1 and consists of a controller card, based upon the LPC2468 microcontroller [17], connected to a remote I/O card through a Modbus-CAN [16] bus. A local I/O device configured as shown in Figure 4 is also part of the setup. Footprint information has been derived from link-time information, while execution performance has been assessed by instrumenting the framework code with timestamping points.

The resolution of the standard FREERTOS time services is limited by the tick timer frequency, which is set to 1 kHz by default and cannot be increased significantly without incurring unacceptable overhead. For this reason, a separate 32-bit hardware counter was used for timestamping, as in [18]. It runs at the same clock speed as the CPU, that is, 72 MHz, thus reaching a resolution of about 14 ns.

Since counter registers are readily accessible to the CPU, timestamping is performed in less than 10 machine instructions, which include storing the timestamp into fast static RAM. The timestamping execution time S was estimated by taking two timestamps consecutively and calculating their difference. Over 2000 samples, the average execution time was found to be $\mu_S = 0.48 \,\mu s$ with negligible variance $\sigma_S^2 < 2.13 \cdot 10^{-4}$.

This estimate might be marginally optimistic, since the compiler might be able to optimize timestamping operations
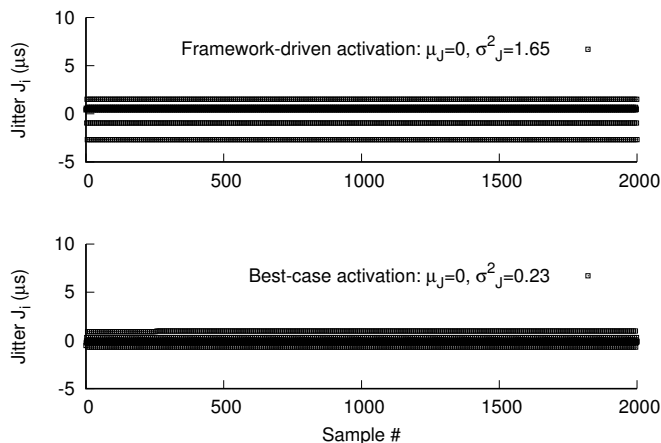
Figure 7. Experimental time traces for control function activation.
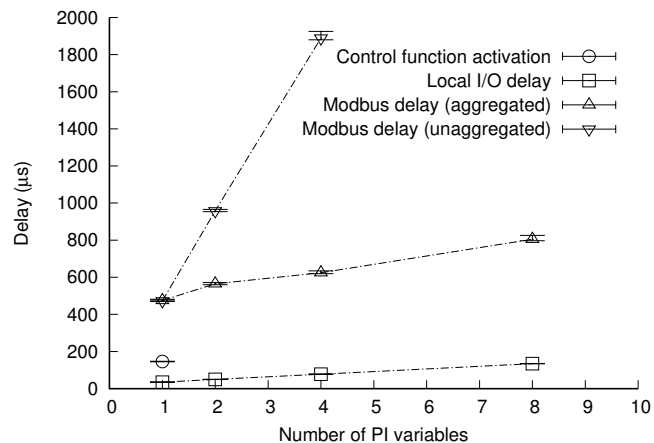
Figure 8. Delays introduced by main framework activities.

better than in other cases, if they are very close to each other. Nevertheless, it confirms that timestamping is not invasive when considering time intervals of tens of microseconds at least. The maximum time interval that can be measured without wraparounds is around $59\,\mathrm{s}$ and static RAM capacity is sufficient to hold up to about 4000 timestamps.

A. Execution Performance and Overhead

Execution performance evaluation revolved around the following two aspects, both related to framework overhead.

1) The ability of the framework to execute the C phase of the control cycle with an accurate *period* and acceptable *jitter*.

2) The *delay* introduced by the main framework activities, as a function of the number of PI variables and the kind of board being used.

For what concerns the first aspect, best-case performance is attained when the C phase is triggered directly by the underlying RTOS timing mechanism, `vTaskDelayUntil` for FREERTOS, without interposing any other software layer. Any difference between this term of reference and the actual framework-controlled C phase activation performance is due to the overhead of the framework itself—more specifically, its even system. Denoting by $c_0, c_1, \dots$ the sequence of *nominal* C phase activation times, equally spaced by the nominal cycle period $P = c_i - c_{i-1}$ $\forall i > 0$, the jitter J_i affecting the i-th C phase can be determined by measuring the sequence of *actual* C phase activation times $c'_0, c'_1, \dots$ and calculating the actual cycle period P'_i of the i-th C phase as:

$$P'_i = c'_i - c'_{i-1} \quad \forall i > 0. \tag{1}$$

Then, J_i is given by the difference between the actual and nominal period of the i-th C phase, that is:

$$J_i = P'_i - P \quad \forall i > 0, \tag{2}$$

where positive values of J_i denote a late activation and negative values denote an early activation. The mean value of J_i over all i (denoted by μ_J) is expected to be zero and any non-zero value indicates a systematic error of the actual periods versus the nominal ones. The variance of J_i (denoted by σ_J^2) represents the jitter magnitude. Experimental results for best-case activation over 2000 samples are shown at the bottom of

Figure 7. They manifest the absence of systematic timing errors ($\mu_J = 0$) and exhibit an activation jitter $\max_i |J_i| < 1\,\mu\mathrm{s}$ with $\sigma_J^2 = 0.23$. The top part of the same figure also shows the activation jitter with the interposition of the framework event system depicted in Figure 6 between the cyclic event source and the control task. The experimental results confirm that the jitter increases to a $\max_i |J_i| < 3\,\mu\mathrm{s}$ with $\sigma_J^2 = 1.65$, but it is still negligible with respect to the minimum cycle period the framework and the underlying RTOS support, that is, $1\,\mathrm{ms}$. At the same time, observing that it is still $\mu_J = 0$ rules out any systematic timing errors the framework might introduce.

Regarding the second aspect under evaluation, Figure 8 depicts the two most important sources of overhead within the framework. Both have been evaluated experimentally and affect the minimum attainable cycle time. Namely:

1) the delay introduced by the event system shown in Figure 6 when activating the control function;

2) the total time needed by the O and I phases depicted in Figure 3.

The second delay has been measured as a function of the number of configured PI variables, also taking into account the kind of board they reside on (local versus remote) and the possibility of aggregating multiple variable updates into a single bus transaction (for remote Modbus boards only). On the other hand, the first delay has been measured only once (and is shown near the bottom left corner of the figure) because it is independent from all those factors. In each plot, the symbol is placed on the mean delay calculated over 2000 samples and whiskers extend to the minimum and maximum measured delay. Only input PI variables have been considered in the experiments, because outputs cause analogous delays.

The results presented in Figure 8 show that the control function activation delay is below $200\,\mu\mathrm{s}$ and is negligible with respect to other delay sources, especially when remote boards are involved. As expected, I/O delays are approximately linear with respect to the number of PI variables. For remote boards, experimental data also confirm that Modbus transactions dominate the delay. On the other hand, I/O delays for local boards provide a reasonable estimate of framework overhead in this area. This is because, in the experimental setup local I/O transactions introduce a negligible amount of delay by themselves and all the rest can be attributed to the

TABLE I. Memory footprint divided by category

Module	Text and RO data (B)	RW Data (B)	BSS (B)
Framework	9938	0	424
Framework Utilities	5044	0	0
Main program	2159	0	228
Local I/O library	260	0	0
Modbus I/O library	26877	0	798
RTOS	16154	8	33052
C runtime library modules	30092	1284	94482
Total	90524	1292	128984

I/O abstraction performed by the framework (see Figure 5). It should also be noted that aggregation brings a significant performance improvement because it trades extra Modbus transactions for a more complex local data processing, at a fraction of the cost. Last, but not least, data are in good agreement with respect to [16]. Any marginal performance improvement in the present case can easily be justified by considering that a faster Modbus slave has been used.

B. Memory Footprint

The same firmware considered in Section IV-A was also evaluated to determine another kind of overhead, that is, its memory footprint. The evaluation was performed statically (on the firmware object code), by means of the `size` toolchain command, leading to the results listed in Table I. The rows of the table correspond to different parts of the firmware, while columns divide footprint into three standard categories: text and read-only (RO) data, read-write (RW) initialized data, and read-write uninitialized data (BSS). These categories are important from the practical point of view because, depending on the target system, they may correspond to different kinds of memory. For instance, text and RO data can conveniently be stored in Flash memory (if available on the target) rather than RAM.

The memory footprint of framework components is given in the first three row of the table. More specifically, we considered:

- the real-time part of the *framework* itself, described in Sections II and III, which also allocates storage for PI variables, as well as their descriptors and states;
- additional *framework utilities*, consisting of functions to dump framework data structures in human-readable format and other debugging aids;
- the *main program*, which allocates the main configuration and board state data structures, besides implementing an exemplar control function.

The rows that follow pertain to other firmware components that are used by the framework, but would be required even without it, namely, the I/O libraries, operating system and C runtime library modules. The results shown in Table I confirm that the framework footprint is acceptable and does not significantly impact overall memory requirements with respect to other major components. Indeed, the total footprint of core components is only 17141 B + 652 B (Text and RO data + BSS), which is lower than the footprint of the Modbus I/O library alone, for instance.

For the sake of completeness, it is worth to remark that the RTOS BSS footprint includes the memory pool from which memory for *task stacks* and all other objects managed by the operating systems is drawn (32 KB). Similarly, the C runtime library BSS includes the library *heap* (64 KB), which

satisfies all dynamic memory allocation requests made by the application code and the library itself, as well as the *other stacks* required by the processor, except task stacks (28 KB).

V. CONCLUSION

This paper presented the design of a firmware development framework whose aim is to speed up application development and deployment with respect to plain C-language programming. The framework has been implemented and its performance experimentally evaluated with satisfactory results, regarding both execution time overhead and memory footprint.

Foreseen future work includes testing the framework in the context of a real-world embedded application, as well as further extending its remote communication capabilities to Ethernet-based networks and protocols.

REFERENCES

[1] M. Samek, Practical UML Statecharts in C/C++, 2nd ed. Newnes, Oct. 2008.

[2] W. Bolton, Programmable Logic Controllers, 6th ed. Newnes, Mar. 2015.

[3] CODESYS, Industrial IEC 61131-3 PLC programming, available online, at https://www.codesys.com [retrieved: Mar. 2017].

[4] T. Strasser, M. Rooker, G. Ebenhofer, A. Zoitl, C. Sunder, A. Valentini, and A. Martel, "Framework for distributed industrial automation and control (4DIAC)," in Proc. 6th IEEE International Conference on Industrial Informatics (INDIN), Jul. 2008, pp. 283–288.

[5] IEC 61131-3, Programmable controllers — Part 3: Programming languages, 3rd ed., International Electrotechnical Commission, Feb. 2013.

[6] Arduino AG, Arduino IDE, available online, at https://www.arduino.cc [retrieved: Mar., 2017].

[7] P. Buonocunto, A. Biondi, and P. Lorefice, "Real-time multitasking in Arduino," in Proc. 9th IEEE International Symposium on Industrial Embedded Systems (SIES), June 2014, pp. 1–4.

[8] ISO/IEC 9899, Programming Languages — C, 3rd ed., International Organization for Standardization and International Electrotechnical Commission, Dec. 2011.

[9] R. Barry, Using the FreeRTOS Real Time Kernel – Standard Edition, 1st ed. Raleigh, North Carolina: Lulu Press, 2010.

[10] ChaN, FatFs Generic FAT File System Module, available online, at http://elm-chan.org/fsw/ff/00index_e.html [retrieved: Mar. 2017].

[11] A. Dunkels, lwIP – A Lightweight TCP/IP stack, available online, at http://savannah.nongnu.org/projects/lwip/ [retrieved: Mar. 2017].

[12] I. Cibrario Bertolotti and T. Hu, "Modular design of an open-source, networked embedded system," Computer Standards & Interfaces, vol. 37, Jan. 2015, pp. 41–52.

[13] C. D. Locke, "Software architecture for hard real-time applications: cyclic executives vs. fixed priority executives," Real-Time Systems, vol. 4, no. 1, 1992, pp. 37–53.

[14] M. Caccamo, T. Baker, A. Burns, G. Buttazzo, and L. Sha, "Real-time scheduling for embedded systems," in Handbook of Networked and Embedded Control Systems, D. Hristu-Varsakelis and W. S. Levine, Eds. Birkhäuser Boston, 2005, pp. 173–195.

[15] T. P. Baker and A. Shaw, "The cyclic executive model and Ada," in Proc. IEEE Real-Time Systems Symposium (RTSS), Dec. 1988, pp. 120–129.

[16] G. Cena, I. Cibrario Bertolotti, T. Hu, and A. Valenzano, "Design, verification, and performance of a MODBUS-CAN adaptation layer," in Proc. 10th IEEE International Workshop on Factory Communication Systems (WFCS), May 2014, pp. 1–10.

[17] LPC2468 Product data sheet, rev. 4, NXP B.V., Oct. 2008, available online, at http://www.nxp.com/ [retrieved: Mar. 2017].

[18] I. Cibrario Bertolotti and T. Hu, "Real-time performance of an open-source protocol stack for low-cost, embedded systems," in Proc. 16th IEEE International Conference on Emerging Technologies and Factory Automation (ETFA), Sep. 2011, pp. 1–8.

5G Candidate Waveforms Comparison Regarding Time-Frequency Resources in the Nonlinear HPA

Heung-Gyoon Ryu
Department of Electronics Engineering
Chungbuk National University
Cheongju, Korea 361-763
e-mail : ecomm@cbu.ac.kr

Abstract - **New waveforms for the 5th generation cellular system have been studied in many ways. The sharper out-of-band (OOB) spectrum characteristics are greatly desired for improving the spectrum efficiency. Generally, universal filtered multi-carrier (UFMC), filter bank multi-carrier (FBMC) and weighted overlap and add orthogonal frequency division multiplexing (WOLA-OFDM) waveforms are regarded as strong waveform candidates for the 5th generation mobile system. Similar to the conventional orthogonal frequency division multiplexing (OFDM) system, these modulation methods use multi-carrier. So, these systems have high peak to average power ratio (PAPR), which can cause nonlinear distortion and the out-of-band (OOB) power will increase because of the nonlinear high power amplifier (HPA). In this paper, we evaluate the spectrum characteristic and bit error rate (BER) performance of the waveforms under the effect of nonlinear HPA. Also, we show the comparison of the time-frequency resources of each system because it is very important to estimate the spectral efficiency and communication throughput. As simulation results, it is confirmed that the OOB power of each system increases, and the OOB power increase of the FBMC system is the largest. We provide the comparison table for the time-frequency resources requirement for the each multi-carrier system.**

Keywords—OFDM; FBMC; UFMC; WOLA-OFDM; HPA nonlinearity

I. INTRODUCTION

Recently, mobile traffic has increased dramatically because the number of various mobile devices and multimedia services has increased [1]. Also, the growth of mobile traffic has accelerated. It is difficult for the present mobile communication system to support the mobile traffic required in the future [2]. In order to solve the problem, studies for next generation 5G mobile communication are being actively carried out [3] [4].

Conventional orthogonal frequency division multiplexing (OFDM) based on multi-carrier has high-power out-of-band (OOB) [5]. This characteristic causes adjacent channel interference (ACI). OFDM uses a wide guard band in order to avoid ACI. It decreases spectral efficiency when a number of mobile devices simultaneously access a base station. Next generation mobile communication system requires high-level key performance indicators (KPIs). It is difficult for OFDM to satisfy the KPIs. Universal filtered multi-carrier (UFMC) and filter bank based multi-carrier (FBMC) are known as the waveform candidates for 5G mobile communication [6] [7]. When the f-OFDM, suggested by Huawei, appeared in the first place, the filtered-OFDM system adopted one-filter system for the sharper OOB spectrum characteristics. However, they changed into the multiple filter system, which became very

similar to the UFMC system. These systems use filtering techniques based on the multi-carrier. These techniques have the characteristic of low OOB power spectrum in comparison with the conventional OFDM. Therefore, these systems have high spectrum efficiency. FBMC uses the filtering technique in each sub-carrier. UFMC uses a filtering technique in each sub-band [8] [9].

However, these systems based on the multi-carrier are vulnerable to non-linearity of high-power amplifier (HPA), like OFDM. OFDM has high peak-to-average power ratio (PAPR) because multi-carrier signals are overlapped. High PAPR causes nonlinear distortion in HPA because it saturates HPA. Similarly, UFMC and FBMC have high PAPR because these systems are based on multi-carrier [10] [11]. In UFMC and FBMC systems, if nonlinear distortion is caused by high PAPR, the OOB power of these systems is increased. That is, the advantage of these systems vanishes. Therefore, this drawback should be overcome in the candidate techniques for 5G mobile communication.

In this paper, in order to overcome the drawback, we focus on the spectrum characteristic analysis and the performance evaluation of FBMC and UFMC systems under the effect of nonlinear HPA. Firstly, we describe and explain OFDM, UFMC, FBMC, weighted overlap and add orthogonal frequency division multiplexing (WOLA-OFDM) system. Then, we design the systems in the linear environment and we analyze the spectrum characteristic of each system and evaluate the bit error rate (BER) performance of each system in this linear condition. Next, we consider the nonlinear condition. So, we analyze the spectrum characteristic and evaluate the bit error rate (BER) performance of each one of the modulation systems under the effect of nonlinear HPA.

Also, we show the comparison of the time-frequency resources of each system because it is very important to estimate the spectral efficiency and communication throughput. We provide the comparison table for the time-frequency resources requirement for the each one of modulation systems.

In Section 2, each candidate multi-carrier system is described and the Saleh model is included for the nonlinear modelling. Simulation parameters are set for the OOB power evaluation and time resource requirement in Section 3. Finally, we conclude this paper in Section 4.

II. SYSTEM MODEL

A. OFDM

In the transmitter of OFDM system, the data symbols are converted into a parallel stream from a series stream by the

serial to parallel (S/P) block. The changed symbols are mapped onto each subcarrier by the inverse fast Fourier transform (IFFT) operation. IFFT operation transforms the frequency-domain signal into time-domain signal. After the IFFT operation, the time-domain signals are converted into the stream by parallel to serial (P/S) block. Then, cyclic prefix (CP) is added in order to reduce the effect of inter-symbol interference (ISI). Next, the base-band signals are applied to the radio frequency (RF) chain. Finally, the RF signal is amplified by high-power amplifier (HPA). The receiver of OFDM system consists of the reverse structure in comparison with the OFDM transmitter. In the OFDM receiver, an equalizer is used to compensate the multi-path effect. Simple one-tap equalizer can be used because of the CP. This is an advantage for the OFDM system. However, each subcarrier of OFDM system has high side-lobe power. Therefore, OOB power spectrum increases, which makes the guard band wider between the information channels. As a result, channel capacity is decreased in the OFDM system [12]. These drawbacks should be overcome for 5G mobile communication.

B. UFMC

The UFMC system also uses orthogonal multi-carrier, like the OFDM system. UFMC filters each sub-band that consists of orthogonal multi-carrier in order to reduce the OOB power [6]. Each sub-band signal is converted into a series stream by the P/S. Secondly, in the UFMC receiver, the received signal is applied to the RF chain. The received signal is transformed into a baseband signal by the RF chain. The baseband signal is converted into digital signal by ADC. Then, time-domain pre-processing is done. After this process, the series data stream is converted into a parallel data stream by S/P. The time-domain parallel data stream is converted to frequency-domain stream by the 2N-FFT operation [6]. After the 2N-FFT operation, odd numbered data symbols are selected and equalized. The spectrum of the UFMC system has lower OOB power in comparison with the spectrum of the OFDM system. This is an advantage. However, because the UFMC system uses multi-carriers and multi-carriers are overlapped, the UFMC system has high PAPR. The high PAPR characteristic can distort the signal of the UFMC system [6].

C. FBMC

The FBMC system uses multi-carrier, too. The FBMC system filters each sub-carrier in order to reduce the OOB power spectrum [7]. In the transmitter of the FBMC system, data symbols are converted into a parallel stream from a series stream by the S/P. The parallel symbols are modulated to offset the quadrature amplitude modulation (OQAM) signal [7]. The modulated OQAM signal is converted into a signal filtered by each sub-carrier by using a synthesis filter bank which consists of IFFT and poly phase network (PPN) [7]. Finally, the amplified FBMC signal is transmitted by the antenna. The receiver of the FBMC system consists of a reversed structure in comparison with the FBMC transmitter. The FBMC system has lower OOB power in comparison with the UFMC system and the OFDM system. This is an advantage. However, the FBMC system has high system complexity. Additionally, because the FBMC system uses multi-carriers, it has high PAPR.

D. WOLA-OFDM

The WOLA-OFDM is an improved version of the OFDM system. Fig.1 shows the WOLA-OFDM system. The WOLA-OFDM system does not use the filter, but it uses the extension and windowing method on each OFDM symbol in order to reduce the OOB power spectrum.
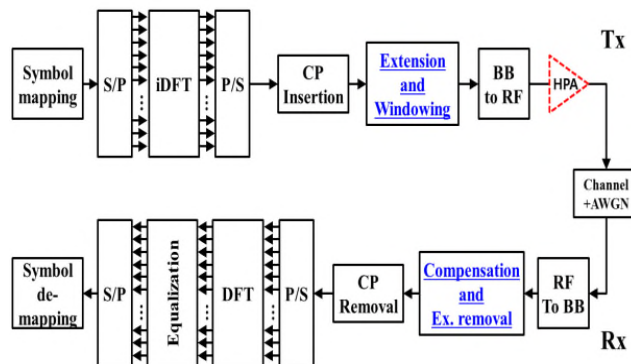
Fig. 1. Block diagram of WOLA-OFDM system.

In this paper, the research purposes are spectrum characteristic analysis and performance evaluation of OFDM, UFMC, FBMC and WOLA-OFDM systems under the effect of nonlinear HPA. Therefore, we have investigated each system including the nonlinear HPA system. The famous Saleh model is used for the nonlinear HPA. The characteristics of AM-AM and AM-PM in the Saleh model are as follows [13].

$$G[A(t)] = \frac{\alpha_A A(t)}{1+\beta_A A(t)^2} \qquad (1)$$

$$\Phi[A(t)] = \frac{\alpha_\Phi A(t)^2}{1+\beta_\Phi A(t)^2} \qquad (2)$$

Equation (1) shows the AM-AM characteristic of the Saleh model for the nonlinear HPA. *A* is the amplitude of input signal. α_A and β_A are coefficients for adjusting amplitude of the output signal. Equation (2) shows the AM-PM characteristic of the Saleh model. α_Φ and β_Φ are coefficients for adjusting phase of the output signal.

III. SIMULATION RESULTS AND ANALYSIS

Table 1 shows the parameters setting for getting the communication performance of each multi-carrier system.

TABLE I.   SIMULATION PARAMETERS

Parameter	Value
Modulation	QPSK
# of total subcarrier	64
# of used subcarrier	32
# of null subcarrier	32
Filter for FBMC	Phydyas prototype : H0 = 1 , H1 = 0.97196 H2 = 0.7071 H3 = 0.235147
Filter for UFMC	Chebyshev : Attenuation = 60dB, Length = 10
# of sub-band in UFMC	64/8
# of used sub-band in UFMC	4

Table 2 shows the parameters setting of the HPA nonlinear conditions. Condition 0 is the linear case. Conditions 1 to 5 are

the nonlinear conditions. Condition 1 is the weakest nonlinear. Condition 5 is the strongest nonlinear.

TABLE II. NONLINEAR HPA PARAMETER SETTING OF SALEH MODEL.

Condition	AM-AM	AM-PM
0 (Linear)	$\alpha_A = 1$	$\alpha_\Phi = 0$
	$\beta_A = 0$	$\beta_\Phi = 0$
Nonlinear 1	$\alpha_A = 1$	$\alpha_\Phi = 0.26$
	$\beta_A = 0.04$	$\beta_\Phi = 15.9$
Nonlinear 2	$\alpha_A = 1$	$\alpha_\Phi = 0.26$
	$\beta_A = 0.2$	$\beta_\Phi = 2.38$
Nonlinear 3	$\alpha_A = 1$	$\alpha_\Phi = 0.26$
	$\beta_A = 0.4$	$\beta_\Phi = 0.69$
Nonlinear 4	$\alpha_A = 1$	$\alpha_\Phi = 0.26$
	$\beta_A = 0.6$	$\beta_\Phi = 0.127$
Nonlinear 5	$\alpha_A = 1$	$\alpha_\Phi = 0.26$
	$\beta_A = 0.8$	$\beta_\Phi = -0.155$

TABLE III. COMPARISON OF OOB POWER CHARACTERISTICS

Condition	OFDM	UFMC	FBMC	WOLA-OFDM
Linear	-26 dB	-83 dB	-120 dB	-90 dB
condition 1	-26 dB	-82 dB	-85 dB	-85 dB
condition 2	-26 dB	-74 dB	-75 dB	-75 dB
condition 3	-26 dB	-66 dB	-67 dB	-69 dB
condition 4	-26 dB	-61 dB	-62 dB	-63 dB

After the simulation using the parameters from Tables 1 and 2, we can get the OOB (out-of-band) power spectrum at the output of the HPA of each system. Table 3 shows the OOB power spectrum comparison for each system. The lower the OOB power, the more desirable it is to set the smaller guard band and finally to increase the spectrum efficiency. From Table 3, it can be confirmed that under the HPA nonlinearity environment, the FBMC system shows the biggest change of OOB power, and the OFDM system shows the smallest change.

Figures 2 to 5 show BER performances of each multi-carrier system. Compared with the linear condition, BER performance of every system is degraded in the nonlinear HPA environment. Importantly, the FBMC system shows the smallest degradation of BER performance. However, even though the FBMC system is the strongest against HPA nonlinearity, every multi-carrier system needs the PAPR reduction method for the nonlinear distortion compensation and power saving.
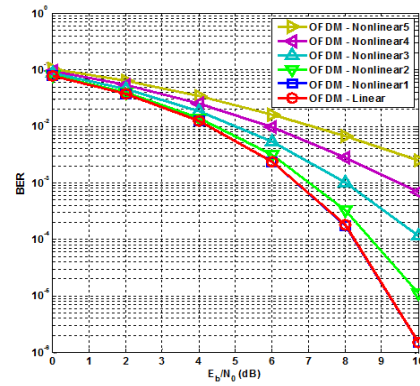
Fig. 2. BER of OFDM system.
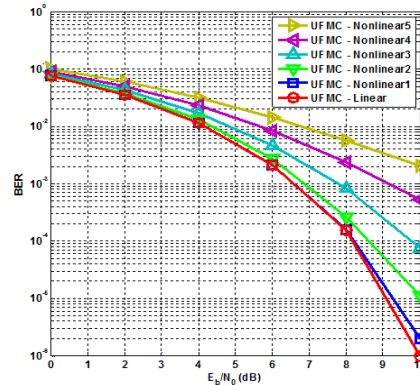
Fig. 3. BER of UFMC system.
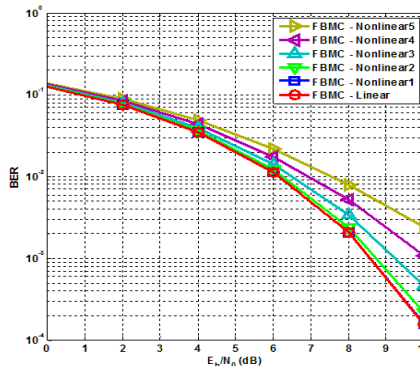
Fig.4. BER of FBMC system.
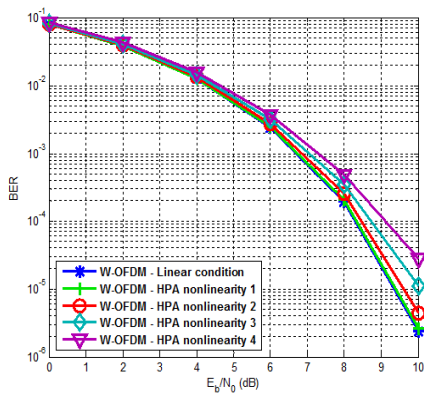
Fig.5. BER of WOLA-OFDM.

Next, in order to compare the time-frequency resources of each multi-carrier system, we have set some necessary parameters conditions for the simulation, as in the below.

Allocated bandwidth : 20MHz

\# of used sub-carriers : 16

\# of transmission bits : 128

4QAM modulation (2bit) * 16 sub-carrier * 4 synthesis symbols : 128 bits

IFFT size : 64, and CP length : 9

FBMC, Overlapping Factor (K) : 4

WOLA-OFDM, Extension length : 6

OOB emission suppression (Frequency, 7.5MHz Offset) / TTI length (Time)

TABLE IV. COMPARISON OF THE TIME-FREQUENCY RESOURCES

	OFDM	UFMC	FBMC	WOLA-OFDM
Linear	-26 dBc / 292	-83 dBc / 292	-130 dBc / 480	-66 dBc / 304
HPA condition 1	-26 dBc / 292	-82 dBc / 292	-85 dBc / 480	-66dBc / 304
HPA condition 2	-26 dBc / 292	-74 dBc / 292	-75 dBc / 480	-66dBc / 304
HPA condition 3	-26 dBc / 292	-66 dBc / 292	-67 dBc / 480	-65dBc / 304
HPA condition 4	-26 dBc / 292	-63 dBc / 292	-65 dBc / 480	-63dBc / 304

After the investigation of OOB spectrum power at 7.5MHz offset frequency from the information signal band and time resource requirement for the above 4-QAM transmission, we can get Table 4 showing the OOB (out-of-band) power and required time resource for each multi-carrier system under several nonlinear HPA conditions. As seen in Table 4, OFDM and WOLA-OFDM have almost no change from the linear case to the nonlinear condition 4. However, UFMC and FBMC have some quite big change from the linear case to the nonlinear condition 4. As in Table 4, OFDM and UFMC systems have the time resource length of 292. WOLA-OFDM system has time resource length of 302. However, FBMC system has the longest time length of 480. So, FBMC requires longer time

resource even though it has very sharp OOB power spectrum in the linear condition.

Even though 4-QAM is used for the simulation and time frequency requirement, the trend would be almost the same when extended into higher modulation levels.

IV. CONCLUSIONS

The FBMC and UFMC systems are strong modulation candidates for 5G mobile communication systems. Since these systems are basically multi-carrier systems, it is important to study the non-linearity sensitivity. In this paper, we have focused on spectrum characteristic analysis and BER performance evaluation of OFDM, FBMC, and UFMC, WOLA-OFDM systems under the effect of nonlinear HPA. As simulation results, we have confirmed that, if the HPA non-linearity rises in each multi-carrier system, the OOB power of each multi-carrier system increases. The OOB power increase of the FBMC system is the biggest. Additionally, we have confirmed that the performance of every multi-carrier system is degraded by the strength of the HPA non-linearity, and every system needs the PAPR reduction method for the non-linear distortion compensation and power saving, even though it would be more complicated. Also, we show the comparison of the time frequency resources of each multi-carrier system because it would be very important to estimate the spectral efficiency and communication throughput. We provide the comparison table for the time-frequency resources requirement for each multi-carrier system.

The next step will be on the system design and evaluation of the PAPR reduction scheme and complexity comparison for the system implementation.

REFERENCES

[1] Shanzhi Chen, and Jian Zhao, "The requirements, challenges, and technologies for 5G of terrestrial mobile telecommunication," IEEE Communications Magazine, vol. 52, no. 5, pp. 36-43, May 2014.

[2] E. Dahlman, G. Mildh, S. Parkvall, J. Peisa, J. Sachs, Y. Selén, and J. Sköld, "5G wireless access: requirements and realization," IEEE Communications Magazine, vol. 52, no. 12, pp. 42-47, December 2014.

[3] G. Wunder et al., "5GNOW: non-orthogonal, asynchronous waveforms for future mobile applications", IEEE Communication Magazine, vol. 52, no. 2, pp. 97-105, Feb. 2014.

[4] Paolo Banelli, Stefano Buzzi, Giulio Colavolpe, Andrea Modenini, Fredrik Rusek, and Alessandro Ugoliniet, "Modulation Formats and Waveforms for the Physical Layer of 5G Wireless Networks: Who Will be the Heir of OFDM?", IEEE Signal Processing Magazine, vol. 31, issue 6, Nov. 2014.

[5] F. Schaich, and T. Wild, "Waveform contenders for 5G - OFDM vs. FBMC vs. UFMC," 2014 6th International Symposium on Communications, Control and Signal Processing (ISCCSP), pp. 457-460, 21-23 May 2014.

[6] V. Vakilian, T. Wild, F. Schaich, S. Ten Brink, and J.F. Frigon, "Universal-filtered multi-carrier technique for wireless systems beyond LTE," 2013 IEEE Globecom Workshops, pp. 223-228, 9-13 Dec. 2013.

[7]   B. Farhang-Boroujeny, "OFDM Versus Filter Bank Multi-carrier," IEEE Signal Processing Magazine, vol. 28, no. 3, pp. 92-112, May 2011.

[8]   Wonsuk Chung, Beomju Kim, Moonchang Choi, Hyungju Nam, Hyunkyu Yu, Sooyoung Choi and Daesik Hong, "Synchronization Error in QAM-Based FBMC System," 2014 IEEE Military Communications Conference (MILCOM), pp. 699-705, 6-8 Oct. 2014.

[9]   Mukherjee, Mithun, Shu, Lei, Kumar, Vikas, P. Kumar, and R. Matam, "Reduced out-of-band radiation-based filter optimization for UFMC systems in 5G," 2015 International Wireless Communications and Mobile Computing Conference (IWCMC), pp. 1150-1155, 24-28 Aug. 2015.

[10] Z. Kollar, L. Varga, and K. Czimer, "Clipping-Based Iterative PAPR-Reduction Techniques for FBMC," 17th International OFDM Workshop 2012 (InOWo'12), pp. 1-7, 29-30 Aug. 2012.

[11] M. Chafii, J. Palicot, and R. Gribonval "Closed-form approximations of the PAPR distribution for Multi-Carrier Modulation systems," 2014 Proceedings of the 22nd European Signal Processing Conference (EUSIPCO), pp. 1920-1924, 1-5 Sept. 2014.

[12] A. M. Elshirkasi, M. U. Siddiqi, and M. H. Habaebi, "Generalized Discrete Fourier Transform Based Minimization of PAPR in OFDM Systems," 2014 International Conference on Computer and Communication Engineering (ICCCE), pp. 205-208, 23-25 Sept. 2014.

[13] P. Drotar, J. Gazda, D. Kocur, and P. Galajda, "MC-CDMA performance analysis for different spreading codes at HPA Saleh model," 18th Int. Conf. Radioelektronika, pp. 1-4, Prague, Apr. 2008.

An Identity-Based Encryption Scheme with Performance Optimization for Privacy Preservation in Smart Grid Communication

Ulas Baran Baloglu

Department of Computer Enginnering

Munzur University

Tunceli, Turkey

email: ulasbaloglu@gmail.com

Yakup Demir

Department of Electrical and Electronics Engineering

Firat University

Elazig, Turkey

email: ydemir@firat.edu.tr

Abstract—**Smart grids are expected to replace existing electrical grids with advanced mechanisms and intelligent entities, which have excessive data processing and communication tasks. It is important for the sensitive consumer data, such as meter readings, to be secured at these intelligent entities. Novel digital communication mechanisms should be developed to protect privacy. Existing smart grid architectures do not have sufficient and efficient security functionalities for data transmission. In this paper, we propose an Identity-Based Encryption scheme, which is more promising than the classical form regarding performance and security. The proposed scheme focuses on the data structure of meter readings and optimizes this structure to achieve a better privacy preservation. This novel structure further improves the performance of the scheme by reducing communication overhead caused by public key creation and distribution operations, as evaluations demonstrated.**

Keywords-identity-based encryption; smart grid; privacy preservation.

I. INTRODUCTION

In the following years, smart grids are expected to replace the classical grids. Advances in information science opened a new path to the grids for transmitting power in a more efficient way than before. The electricity grids are going to be equipped with adaptation mechanisms, control technologies, data processing systems and communication mechanisms to react to various grid problems. Problems, such as power quality, will still exist in smart grids as they did in the past, but the grid structure will be more robust and efficient. The biggest problems with the transition to smart grids will be information security based including computation, data communication, and storage. Therefore, privacy and data security will play a very crucial role in the success of future smart grids.

Smart grids add the complexity of a communication layer to an electric power system, which is already a complex physical network. The introduction of this layer may create new challenges, especially regarding security. Smart meter readings may reveal some private information about daily lives and routines of its consumers. As a result, smart meters have to fulfill four essential security requirements: data authenticity, data confidentiality, data integrity and consumer

privacy [1][2]. These requirements can be achieved by sender authentication, communication security, and privacy preservation techniques. Every part of a smart grid infrastructure must incorporate at least some fundamental cryptographic features to perform tasks such as data encryption and authentication [2].

There are several studies in the literature aiming to protect consumer privacy while fitting with the smart grid concept. One way of doing this is encrypting metering data before transmitting it. For this purpose, various encryption schemes are applied in this field such as ElGamal encryption system, which outperforms existing schemes based on Paillier's homomorphic cryptosystem [3]-[6]. This encryption system is secure under chosen plaintext attacks (CPA), but it is not secure under chosen ciphertext attacks (CCA) [6]. Boneh-Goh-Nissim is another homomorphic encryption technique, which has one multiplication between an arbitrary number of additions [7]. These studies are typically directed towards developing a cryptography system so that they have not paid much attention to whether they are suitable for smart grids.

Other studies prefer to perturb meter readings, which is defined as a process for adding noise to hide the true meter readings or privacy of consumers while preserving the usability [8]. There are several types of perturbation, such as adding noise (additive perturbation), k-anonymity, compressing data, differential privacy, and geometric transformation [9]-[11]. Bayes Estimate and Principal Component Analysis can also be used for perturbation purposes [12]. The main problem of perturbation techniques is the removal of noise from data, which is a difficult and computationally expensive task. Furthermore, intruders can steal perturbed data and statistically analyze it to reveal a consumption profile.

Although there exist some studies about preserving privacy in smart metering systems by applying Identity-Based Encryption [13]-[16], there are some significant differences between those studies and the proposed scheme. Our study differs from the previous studies by focusing on the data structure of the meter readings. It helps us to increase the security while preserving privacy by separating identity information from the metering data. Another contribution of this study is the performance optimization. Unlike all other previous studies, encryption is not

performed by using the user identities separately; instead, timestamp values of the meter readings used. Using a common timestamp value avoids a lot of key circulation inside the system, and computations can be done collectively instead of computing every key individually because all meters have the same timestamp value when the readings are completed.

The rest of this paper is organized as follows. In Section II, we explain preliminaries that are used to construct the proposed scheme. Section III describes the entities of the scheme, and in Section IV, the efficiency is evaluated. We finally conclude the paper in Section V.

II. PRELIMINARIES

In this section, we briefly outline the cryptography primitives that serve as a basis to describe the proposed privacy-preserving scheme.

A. Bilinear Pairing

Bilinear pairing is defined by a quintuple $<p, G_1, G_2, e, g>$ [13]. In this technique, G_1 and G_2 are two cyclic groups with the same prime order denoted as p. The generator of G_1 is denoted with g, and the efficient bilinear map is defined as $e : G_1 \times G_1 \to G_2$ such that $e(g^a, h^b) = e(g, h)^{ab}$ for every $g, h \in G_1$ and $a,b \in Z^*_{(p)}$. This bilinear map is proved to be non-degeneracy and computationally polynomial [13].

B. Identity-Based Encryption for Smart Meters

Identity-Based Encryption scheme derives public keys from public identities, such as e-mail addresses instead of using certificates and it is an important alternative to certificate-based key infrastructures. Figure 1 demonstrates this scheme and how it eliminates usage of certificates. In this scheme, a consumer encrypts a meter data with a public key, for example with a meter id, and then transmits it to an aggregator. Later, the aggregator collects the private key from the private key generator to decrypt the transmitted data. In this scheme, participants can encrypt data with no prior distribution of keys, which could be a problematic issue for smart meters.

BasicIdent is an identity-based encryption algorithm, which contains four separate algorithms: setup, extract, encrypt and decrypt [13]. In this algorithm, there are two cyclic groups G_1 and G_2, and three random generators are chosen as $R_1, R_2, R_3 \in G_1$. Two hash functions are defined as $H_1 : \{0, 1\}^* \to (G_1)^*$ and $H_2 : G_2 \to \{0, 1\}^*$. A random value s is chosen to be the master key, and it is used to calculate the public key as $P_{pub} = sR_1$ where $s \in Z^*_{(p)}$.

In the proposed scheme, smart meters receive their secret keys by using their meter identification number. Public keys of smart meters are calculated as $SM_p = H_1(SM_{ID})$, and these values are used to produce secret keys $SM_s = s(SM_p)$. These keys are sent to the metering devices and the aggregator. Smart meters receive their secret keys by using their meter identification number.
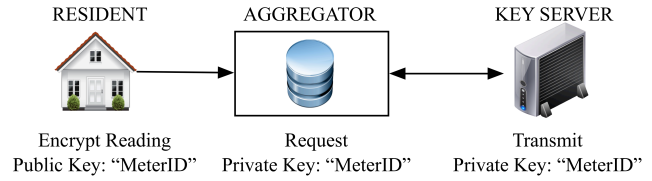
Figure 1. Identity-Based Encryption scheme.

The meter readings $(M_{ID})^t$ are signed with the pair $\Gamma(U,V)$ by first selecting a random number $k \in Z^*_{(p)}$. It is used the calculate $U = kR_1$ and $V = SM_{ID} + kH_2(ID, (M_{ID})^t, U)$. The verification is based on the value $e(R_1, V)$. If it is equal to the value of $e(P_{pub}, H_1(ID))e(U, H_2(ID, (M_{ID})^t, U))$ the message is verified, otherwise it is rejected.

C. Problem Definition

The problem can be defined as transmitting smart meter readings in a secure way to a smart grid application server to be used in other smart grid applications, such as demand management systems. Each smart meter records readings at predetermined intervals t. There are 96 records in total to be transmitted per day when the value of t is chosen as 15.

For this study, we have the following assumptions:

- We assume that the internal hardware of metering devices is not accessible. This study concentrates on transmission security and data privacy.
- We assume that each metering device operates independently.
- Finally, we assume that the application server is in a safe zone. Server security mechanisms are beyond this study's interest.

III. THE PROPOSED SCHEME

The proposed privacy-preserving aggregation scheme for secure smart grid communications is based on Identity-Based Encryption [13]. However, the proposed scheme has some different aspects, as it shown in Figure 2. The scheme mainly consists of the following five entities: residents, id collector, key server, aggregator, and application server.

Residents are the consumers with smart metering devices. The scheme can also be applied with an extended-star topology by limiting the number of users per aggregator. A corrupted or modified device only reveals its individual reading and has no effect on the overall system. Unlike some other methodologies, the scheme does not need any communication between metering devices, and this will reduce communication complexity.

ID Collector collects meter readings from the residents and transmits public keys to them. After collecting the metering data, it stores consumer IDs in a hosted database and modifies the data structure by removing the ID field from the data and then adding a rowID field and data instead. This entity has two type of transmissions, as shown in Table I. The first transmission is forwarding the modified data to the aggregator. The second transmission is as a reply to the queries of the application server.
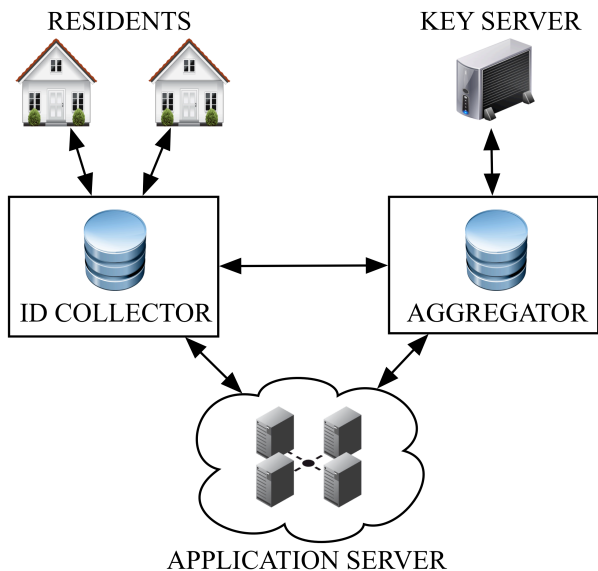
Figure 2. The proposed encyrption scheme.

Sender	Transmission	Receiver	Storage
Residents	(timestamp, ID, Meter Reading)	ID Collector	-
ID Collector	(timestamp, rowID, Meter Reading)	Aggregator	(rowID, ID)
ID Collector	(rowID, ID)	Application Server	-
Aggregator	-	-	(timestamp, rowID, Meter Reading)
Aggregator	(timestamp, rowID, Meter Reading)	Application Server	-

Figure 3. Total computation overhead.

The Aggregator is the entity where the decrypt operation happens. It collects meter readings and divides them into three parts as timestamp, rowID, and reading. For each data collection, only one timestamp value is used for the private key request. All meter readings are decrypted with this private key. After the decryption process, meter readings are stored in a database inside the aggregator. According to the structure of the proposed scheme, this entity has the meter readings but does not know to whom a particular reading has belonged.

Key Server is the private key generator, and it is responsible for key generation and distribution operations. Private keys need to be generated only once. According to the load, there might be more than one aggregator, and the key server in the system and additional servers can be distributed to different geographical locations. Unlike previous studies in the literature, the key server only communicates with the aggregator. Isolating the key server and limiting its accessibility provides a much better security.

Finally, an application server exists for smart grid operations, such as demand management. This server communicates with ID Collector and Aggregator entities to fetch consumption data of the residents. As it seen in Table I, the application server is the only entity, which can access a user's consumption data so that it is accepted as secure and protection of this structure is out of this study's scope.

IV. EVALUATION

In this section, we analyze the security properties and the performance of the proposed scheme.

A. Security

The proposed scheme has all security measures of Identity-Based Encryption scheme [12] since it is originated from that study. As a result, the confidentiality and integrity of the consumers' data are achieved in this study.

Further, the proposed scheme is more secure to the CCA attacks than the classical scheme. A scheme is 'CCA-secure' if access to the decryption oracle does not give valuable information to the attacker. If an attacker somehow gains access to transmit a random message to the key server, the only information resolved will be a meter reading with no consumer information as the consumer information is stored in the ID collector entity. Hence, the privacy of the sensitive data is also achieved in the proposed scheme.

B. Performance

In this subsection, we will evaluate the proposed scheme regarding the computational performance. Figure 3 shows the total computation overhead of the proposed scheme and the traditional Identity-Based Encryption scheme. Total computation overhead is linear to the number of smart meters. The proposed scheme showed a better performance due to two reasons: one key usage for every new time interval and possibly decreased communication overhead. When the number of consumers and keys is small, both the computational and communicational overhead is low in both schemes. Total computation overhead increases with the increased number of smart meters, and this increase is much faster in the case of the traditional scheme. An increase in the number of smart meters also increase the performance losses of the traditional scheme because of the growing number of key exchanges.

It should be noted that an increase in hardware may lower the difference between two schemes but may also cause an excessive increase in the infrastructure costs.

V.   CONCLUSION AND FUTURE WORK

In this paper, we proposed an Identity-Based Encryption scheme for privacy preservation in smart grid communication. Identity-Based Encryption scheme does not have issues, such as certificate lookup and management so that it is preferred in smart grid studies. The proposed scheme is more computationally efficient than the previous methods, and further improves the privacy and the security of the traditional key management infrastructures. The existing studies in the literature have usually been focused on the encryption algorithms themselves, but not on improving their efficiency in particular environments, such as smart grids. In this study, we concentrated on the data structure of meter readings and optimized that structure to make it more appropriate for smart metering systems. The overall performance is improved by reducing communication overhead caused by public key creation and distribution operations.

For future work, we will extend this study to analyze the communication overhead. We would also plan to optimize the computational overhead of the proposed scheme by modifying the encryption algorithm according to the developed data structure.

REFERENCES

[1]   K. Sharma and L. M. Saini, "Performance analysis of smart metering for smart grid: An overview," Renewable and Sustainable Energy Reviews, vol. 49, pp. 720-735, Nov. 2014, doi:10.1016/j.rser.2015.04.170.

[2]   W. Wang and Z. Lu, "Cyber security in the smart grid: Survey and challenges," Computer Networks, vol. 57, pp. 1344-1371, Jan. 2013, doi: 10.1016/j.comnet.2012.12.017

[3]   N. Busom, R. Petrlic, F. Sebe, C. Sorge, and M. Valls, "Efficient smart metering based on homomorphic encryption," Computer Communications, vol. 82, pp. 95-101, May 2016, doi:10.1016/j.comcom.2015.08.016.

[4]   T. E. Gamal, "A public key cryptosystem and a signature scheme based on discrete logarithms," in International Cryptology Conference Advances in Cryptology (CRYPTO), 1985, pp. 10-18.

[5]   P. Paillier, "Public key cryptosystems based on composite degree residuosity classes," In Proceedings of Eurocrypt '99, pp. 223-238.

[6]   X. Dong, J. Zhou, K. Alharbi, X. Lin, and Z. Cao, "An ElGamal-Based efficient and privacy-preserving data aggregation scheme for smart grid," Globecom 2014 Wireless Networking Symposium, pp. 4720-4725.

[7]   D. Boneh, E. Goh, and K. Nissim, "Evaluating 2-dnf formulas on ciphertexts," in Proceedings of Theory of Cryptography, 2005, pp. 325–341.

[8]   F. Laforet, E. Buchmann, and K. Böhm, "Individual privacy constraints on time-series data," Information Systems, vol. 54, pp. 74-91, Dec. 2015, doi:10.1016/j.is.2015.06.006.

[9]   S. K. Hong, K. Gurjar, H. S. Kim, and Y. S. Moon, "A survey on privacy preserving time-series data mining," In 3rd International Conference on Intelligent Computational Systems (ICICS'2013), pp. 44-48.

[10]   X. Yang, X. Ren, J. Lin, and W. Yu, "On Binary Decomposition based Privacy-preserving Aggregation Schemes in Real-time Monitoring Systems," IEEE Transactions on Parallel and Distributed Systems, 27(10), pp. 2967-2983, Jan. 2016, doi: 10.1109/TPDS.2016.2516983.

[11]   P. Barbosa, A. Brito, and H. Almeida, "A Technique to provide differential privacy for appliance usage in smart metering," Information Sciences, vol.370-371, pp. 355-367, Nov. 2016, doi:10.1016/j.ins.2016.08.011

[12]   Z. Huang, D. Wenliang, and B. Chen, "Deriving private information from randomized data," In Proceedings of International Conference on Management of Data, ACM SIGMOD, 2005, pp. 37-48.

[13]   D. Boneh and M. K. Franklin, "Identity-Based Encyrption from the Weil Pairing," In Proceedings of 21st Annual International Cryptology Conference Advances in Cryptology (CRYPTO), Springer, 2001, pp. 213-229.

[14]   J. L. Tsai and N. W. Lo, "Secure Anonymous Key Distribution Scheme for Smart Grid," IEEE Transactions on Smart Grid, 7(2), pp. 906-914, March 2016, doi: 10.1109/TSG.2015.2440658

[15]   H. K. H. So, S. H. M. Kwok, E. Y. Lam, and K. S. Lui, "Zero-Configuration Identity-Based Signcryption Scheme for Smart Grid," 2010 First IEEE International Conference on Smart Grid Communications (SmartGridComm), 2010, pp. 321-326.

[16]   J. B. Hur, D. Y. Koo, and Y. J. Shin, "Privacy-Preserving Smart Metering with Authentication in a Smart Grid," Applied Sciences, vol. 5, pp. 1503-1527, Dec. 2015, doi: 10.3390/app5041503.

A Novel Smart Grid Device Location Mapping Technique

Jim Shima

Qualcomm

Denvor, CO USA

Email: jshima@comcast.net

Stan McClellan

Ingram School of Engineering

Texas State University

San Marcos, TX USA

Email: stan.mcclellan@txstate.edu

Wuxu Peng

Department of Computer Science

Texas State University

San Marcos, TX USA

Email: wuxu@txstate.edu

Abstract—We propose a technique to accurately and quickly determine and resolve the geo-spatial and logical location of grid-resident devices. The technique compare downstream current profiles (DCP) with the superposition of current profiles at the substation (UCP) in the grid. Since small amounts of noise current and perturbations will show up at the substation due to active devices on the grid, the electrical location of each meter can be determined by comparing passive line data from the meter location (DCP) against all the substation feeder lines (UCP). The significance of this approach is that it is *passive* and *efficient* as it does not require additional hardware or communication signals to be introduced to grid infrastructure. The technique can be integrated into current grid systems and implemented using existing smart meter data acquisition facilities and computer/software processing at the utility's datacenter.

Index Terms—Grid, Smart Grid, Grid Devices, Device Location, Geo-Spatial/Physical Location, Electrical/Schematic Location, Device Location Detection, Disturbances

I. Introduction

Electric power distribution networks ("the grid") are a critical and integrated part of modern society. Recent advances in telecommunications and Internet technologies are transforming traditional power distribution grid to *smart grid*, where electric meters can be read and reading sent to a datacenter and operations of the grid can be monitored and controlled in real time through grid control centers [1].

Location information of devices in the grid is critically important [2]. Defining and detecting the *location* of a device in the grid is a fundamentally important capability of the grid. This capability would seem to be obvious or simple given modern technologies of global positioning (GPS), network-based tracking of computer systems, and so on. However, *location* in the grid has at least two independent components: (a) geo-spatial or physical location, and (b) electrical or schematic location. Interestingly, the data which is used to define these components in the grid may be difficult to accurately determine, and effective correlation between the components may be difficult to achieve. For example, even in today's *Smart Grid* [1], utility companies are unable to definitively map a device such as a *smart meter*, to an exact electrical location in the distribution grid. Further, the geo-spatial location of grid-resident devices (which can be resolved via GPS, etc.) may not accurately reflect their electrical

location. Conventional devices *downstream* from a substation are deployed in a fixed location, on a specific feeder, lateral, and phase. However, deviations between the initial design of the system (as-designed), the initial deployment of the system (as-built), and the present configuration of the system (as-modified) often create ambiguities between the geo-spatial and electrical location of particular grid-resident devices.

These ambiguities are problematic, and can be difficult to resolve without significant manual intervention and expense. Up to date, immediately validated knowledge of the feeder, lateral, and phase for grid-resident devices can provide essential feedback to the utility company regarding important grid attributes, such as the aggregate loading of specific circuits or phases, the location and health of sub-circuits and devices, and the presence or absence of load activity. This type of information may become increasingly important as large, mobile source/load devices such as electric vehicles are introduced to the Smart Grid.

Therefore, a technology which could provide automatic reconciliation between physical location and electrical location of grid-resident devices, and in doing so create an accurate, constantly updated *map* of the grid, would be extremely valuable to electric utilities. This paper describes an approach to accurately and quickly determining and resolving the geo-spatial and logical location of grid-resident devices. The significance of this approach is that it is *passive* because it does not require additional hardware or communication signals to be introduced to grid infrastructure. The technique can be implemented using existing smart meter data acquisition facilities and computer/software processing at the utility's datacenter [3], [4], [5].

The rest of the this paper is organized as follows. In Section II we discuss smart meters and issues in grid mapping. We argue that the current grid mapping schemes are inadequate. We review and discuss some fundamentals of smart meters and grid mappings in Section III. We present some critical observations and discuss some important properties and requirements of grid mapping. The core of the paper, an architecture for mapping device locations passively and intelligently, is presented in Section IV. We show how to obtain device location accurately in the presence of noise and disturbances. Summary and concluding remarks are given in
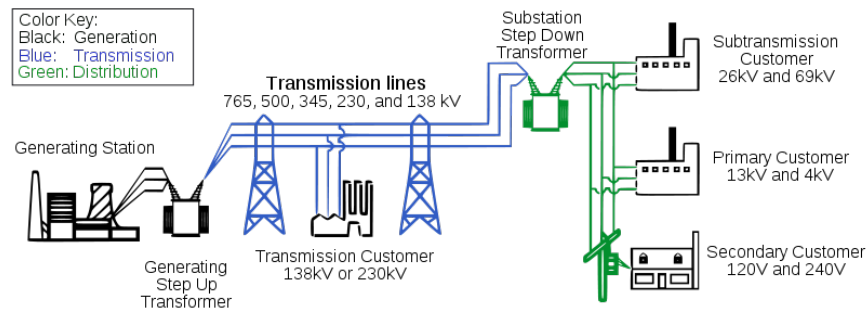
Fig. 1. Grid: Generation, Transmission, and Distribution of Electric Power

Section V.

II. SMART METERS AND GRID MAPPING

Smart meters are fundamental components of smart grids. From the utility's perspective, smart meters allow for remote billing and automatic, network-based retrieval of electrical meter data. This type of Automated Meter Infrastructure (AMI) is more economical than periodic manual reading of electric meters. However, smart meters typically rely on a wireless network to transport meter data to a central location. The use of such extrinsic networks results in significant ambiguity between the physical location of the meter and its electrical location (i.e. *feeder, lateral, phase*).

The reconciliation between a device's geo-spatial location and its electrical location can be referred to as its *grid location*. The geo and electrical location of each meter may have been logged during installation, resulting in a static or *as-built* map of the grid. However, the upstream electrical connections are often changed during outages or seasonal load balancing, destroying important information regarding actual grid connectivity, and resulting in an *as-modified* configuration. Furthermore, older or manual logs of equipment location and circuit architecture may have been inaccurate, resulting in differences between the as-designed and as-built perspectives. Clearly, this situation may have been exacerbated by the realities of several subsequent as-modified conditions.

Additionally, in the present model of system management for the distribution grid, service failures are determined primarily via customer feedback (i.e. phone calls from customers reporting outages.) Utility technicians must then search for the area where the problem occurred by correlating customer feedback with sometimes outdated or otherwise inaccurate schematics of the local grid. If electric service providers had a way to automatically resolve the geo and electrical location of every device on their grid, it would allow them to maintain a constantly up-to-date *grid map* without manual intervention, and even in the face of multiple changes in downstream devices or grid architecture. For example, the installation of new meters would automatically refresh the grid map via communication with the central office, or the re-connection of upstream links after an outage would be automatically reconciled in the centrally-located grid map. In a more complete instantiation of this automated mapping capability, additional communication systems, such as smart transformers, voltage regulators, and the like, could also augment the grid map via targeted or scheduled updates.

An electrical map of the grid requires knowledge of the specific feeder, lateral, and electrical phase where the device resides. For example, as shown in Figure 1, feeders are typically 3-phase, medium-voltage links (13-30kV) which begin at the substation bus and traverse several miles of local distribution territory. In rural settings, feeders can be 50 miles in length and may service hundreds of loads. In urban settings, feeders may be 5-10 miles in length, and may service several thousand loads. Lateral lines branch off from a feeder at downstream locations, and may be 3-phase or 1-phase links which terminate in a distribution transformer. Distribution transformers typically service 3-10 loads, where a load may be a residence or business with an electrical meter. Electrical service to a residence is typically a single-phase link taken from the 3-phase feeder which began at the substation servicing the residence. Clearly, the feeder, lateral, and phase data for a particular load or device are dependent on the actual physical construction of the distribution network at any point in time. Thus, correlation between physical & electrical activity at the substation and physical & electrical activity at the load is a critical factor in the *grid mapping* process.

III. PROBLEMS AND OBSERVATIONS

A substation is a distribution point for medium voltage (MV) electrical service which has been converted from a high voltage (HV) transmission/generating plant. The MV is distributed over the local distribution grid, and converted to low voltage (LV) at the endpoints. The LV power is used in households, commercial buildings, etc. This network architecture is illustrated for reference in Figure 1. In the figure, the distribution grid is shown by the green line segments. Note that a single substation, shown by the junction between blue and green segments, may actually service a distribution grid composed of several thousand loads of various sizes.

A. Distribution Grid

The distribution grid is a complex, time-varying system. The spectra of voltage, current, and impedance all change in real time based on load and activity profiles [6]. As a
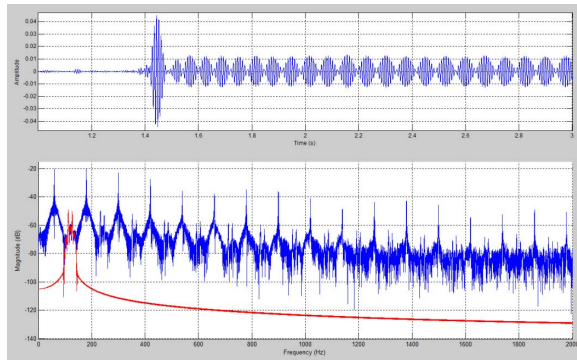
Fig. 2. Example of signal anomalies in the electric distribution grid. This figure shows the time and frequency (magnitude) representation of the turn-on current transient of a television set. The highlighted signal in the spectral plot(bottom) is the anomaly, which due to system characteristics is recursively replicated at 120Hz spacings.

result, the signal environment of the LV power line is very dirty. It contains a large voltage at the fundamental frequency (50Hz in Europe, etc. or 60Hz in the U.S.) as well as odd and even harmonics of this frequency. The LV system also contains non-stationary noise from other connected loads and sources. For example, large electric motors create anomalies at collections of frequencies related to their angular velocity, or large appliances create correlated noise bursts during specific operational events. An example of such a noise burst is shown Figure 2, which shows the turn-on current transient of a television set, as seen from the electric meter. In the figure, time-based and frequency-based artifacts are clearly evident for several seconds as the power supply of the appliance boots up and the system begins operation.

B. Disturbances

Figure 3 contains an alternative perspective of the turn-on transient of the television set. In this figure, a spectrogram is used to jointly analyze time and frequency anomalies. In the bottom section of the figure (a spectrogram), the spectrum of the unfiltered current signal is shown on the vertical axis between 0 Hz and 2000 Hz, and the signal evolves over time along the horizontal axis for roughly 13 seconds. The time-domain perspective of the signal is shown in the top section. During this 13-second period, the TV set was turned on (0 sec), allowed to stabilize (2-10 sec), and then turned off (11 sec). The bottom section of the figure clearly shows stable even-harmonic features during the time that the TV is on and the lack of these same features during the time that the TV is off. Referring to Figure 2, the instantaneous spectral shape of the features is evident (and highlighted) as two closely-spaced peaks near 120 Hz and 25 dB down from the 60 Hz fundamental and 3rd harmonic. A collection of specific features of the time envelope and spectral envelope of these anomalies is tantamount to a digital fingerprint of the power supply for the TV system.

In the case of the TV power supply, the even harmonics contain a clearly recognizable and stable pattern which is noted

on in Figure 3 by *Artifact 1*. In addition to Artifact 1, the TV current transient exhibits multiple temporal frequency artifacts, the most prominent of which is a downward-sweeping chirp near the beginning of the excitation period. This feature is labeled *Artifact 2*. Each of these artifacts contains consistent and easily recognizable features. Further, since the turn-on transient is created by the inrush of current while the system's power supply boots up and engages other system components, the features of this current disturbance travel backwards along the power line, toward the substation. In the process, the signal features can be easily acquired, extracted, compressed, and transmitted to the service provider's datacenter for analysis and comparison with attenuated and obscured current disturbances which are acquired at the substation or other upstream location.

C. Meter Reading and Data Collection

Contemporary deployments of Smart Grid systems collect electricity usage from the consumer's meter and pass that information to a datacenter owned by the service provider or utility [3]. The network system which collects and transports this utilization data is commonly called an AMR/AMI system (automatic meter reading/advanced metering infrastructure) [7]. A generic architecture of an AMR/AMI system is shown in Figure 4. Data collected from the meters may be transmitted via one or more data networks, using unlicensed wireless spectrum (e.g. WiFi, RF aggregators, etc.), licensed wireless spectrum (e.g. cellular telephony), or some form of wired network (e.g. private fiber optic links, conventional power line communications, etc.). In this paradigm, the physical location of the meter is assumed to stay constant after installation, and the electrical location of the meter is derived from static logs and schematic drawings, which can be incomplete or inaccurate (as previously described).

Regardless of the data communications mechanisms for AMR/AMI data, it has been shown that current disturbances which occur *downstream* from the substation (e.g. at the meter) can be detected *upstream* at the substation. For example, the TV data of Figure 3 and Figure 4 was collected upstream of the actual location of the system. This upstream flow of electrical current allows a unique signal, originating from a given meter, to be easily detected at the serving substation. Of course, only signals with frequency content which passes through all the transformers on the feeder are detectable, since higher frequencies are filtered out by the inherent low-pass nature of large series inductors, such as transformers.

For instance, the TV data in Figure 4 is dominated by low-frequency features or artifacts, such as the odd harmonics at multiples of 120Hz (Artifact 1) and the chirp (Artifact 2) which contains significant activity and amplitude below 1000 Hz. At the substation, HV is converted to MV through step-down transformers that lower the voltage but increase the current. As electrical power is distributed through the feeders and to the loads, downstream distribution transformers reduce the voltage from several thousand volts to several hundred volts. This process maintains constant power, and as
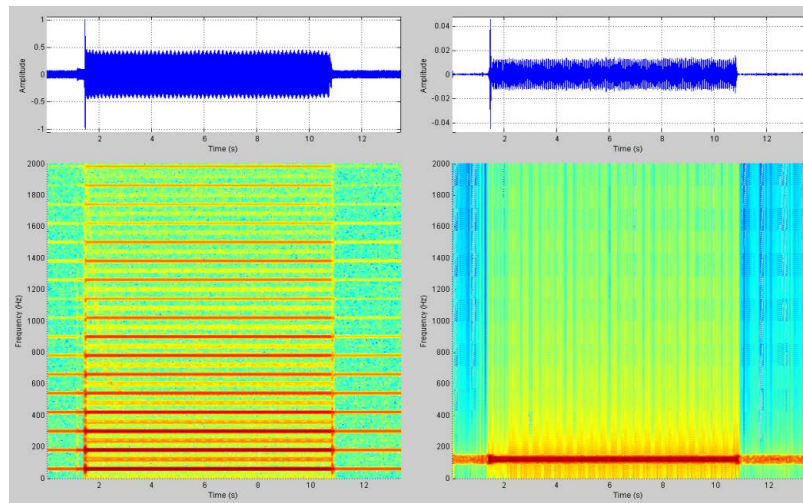
Fig. 3. Time-domain plot and spectrogram of TV turn-on current transient, with artifacts.

a result downstream current must increase. Looking at this system backwards from the endpoint (smart meter) toward the substation, disturbances in the LV-side current that flows upstream must be reduced by the aggregate turns-ratio of the intervening transformers on the feeder. This situation is described graphically in Figure 5. This physical reality causes the distribution grid to behave as a very stable and predictable current attenuator for current disturbances which flow upstream, or from the meter toward the substation. For example, a substation that operates at an MV of 38.4kV and delivers 120V to the consumer has an effective turns-ratio of 1:320. So, a current disturbance created at the meter would show up at the substation with amplitude of approximately 3% (1/320th) of its initial value, assuming no other losses. Thus, a current disturbance with amplitude of 10A at the meter will be detectable at the substation with amplitude of approximately 31mA. In this fashion, recognizable features of all current perturbations in the distribution grid propagate towards the substation. Of course, this propagation is subject to additional noise in the system and the native attenuation characteristic of the distribution transformers. This phenomenon is true for current signals which are purposefully injected (such as communication signals), and it is true for current disturbances which are caused natively or accidentally by all other grid-resident devices.

In the above example, 97% attenuation of a signal appears to be quite problematic. However, studies have shown that even low-level signals with recognizable features are readily detectable at the substation. In fact, current disturbances with attenuation over 99% of the initial amplitude can be detected at the substation. The frequency content of the disturbance is important, as there is a time-varying window of frequencies on every distribution grid which are amenable to good transmission. For example, low-frequency signals (below 400Hz) are swamped by the low-order power line harmonics and resonances from lumped reactive elements on the line, and higher

frequency signals (above 3000Hz) are often filtered out by the aggregate low-pass effect of power transformers and other system characteristics. However, current disturbances with frequency content between 200Hz and 3000Hz are transported directly and predictably towards to substation bus, through intervening distribution transformers, and in spite of additive or time-variant noise due to other grid-resident devices.

IV. PASSIVE AND EFFICIENT LOCATION MAPPING

Current disturbances which are detected at the substation can be used in conjunction with features of current disturbances observed at the meter (or other endpoint) to determine the "electrical location" of grid-resident devices. The correlation/coherence of signals and/or signal characteristics at both points produces a unique feature set which can be used to determine which feeder, phase, and lateral to which the device is attached. When this information is used in conjunction with geo-spatial information from the set of meters which initially detected the disturbance, the *grid location*, which includes electrical and spatial location of the device that caused the disturbance, can be extracted. This feature set approach is valid because all the devices on the grid create a *super signal* that is highly dependent on their locations. Thus, the direct path from the meter location to the substation must produce the best correlation of signals. Crosstalk signals from feeder to feeder, or phase to phase lines, will experience phase and time shifts due to the extra electrical length and additional transformer couplings (on the high side) this phenomenon reduces the effective correlation between the signals, and emphasizes the correct electrical location of the device. The fact that the line fundamental is 120-degrees out of phase on each per-phase link means that the feature correlation task can also be viewed as a best-fit classification problem over a time-varying channel. Consider a substation with 4 feeders distributing electricity to a neighborhood as shown in Figure 6:

At the substation, current transformers (CT) are installed to measure the current signals present on each feeder. These
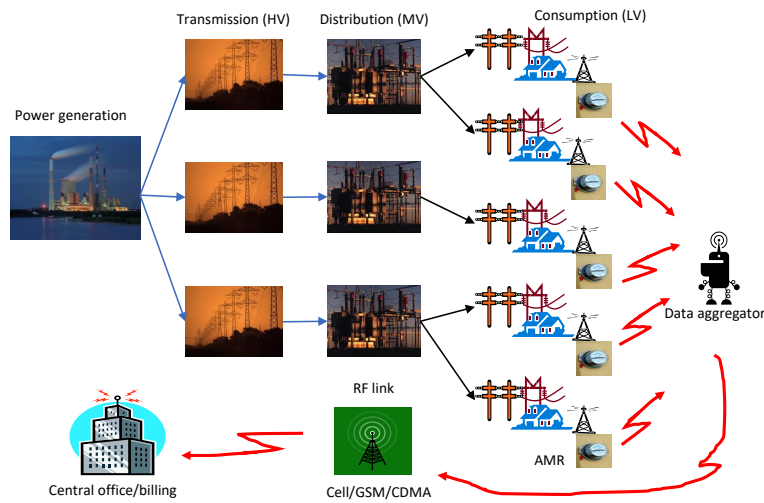
Fig. 4.   Typical AMI backhaul architecture via cellular network.
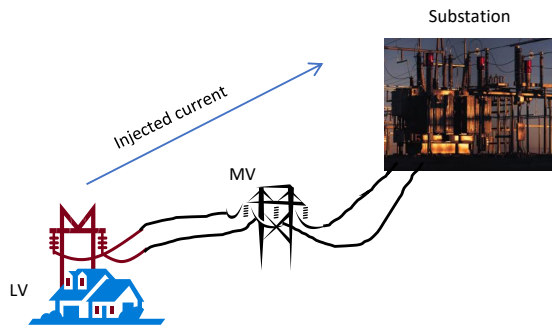
Fig. 5.   Current attenuation in the distribution grid.

current waveforms (or upstream current profiles, UCP) are sampled, time-stamped, and stored in a computer present at the substation or the service provider's datacenter. At each smart meter, the local current signal (or downstream current profile, DCP) is sampled, time-stamped, processed, and transmitted along with the AMR/AMI meter data to the utility datacenter. The computer containing the UCPs also receives the DCPs from each meter. By aligning time stamps on the DCP and UCP data, the substation computer can compare all permutations of feeder and phase between the UCPs and DCPs. The resulting *best match* between DCP and UCP is flagged as the actual feeder/phase where the endpoint meter is located. Mathematically, this can be viewed as a maximization computation over a set of signal features, and is a common processing task for signal comparisons. For example, automatic target recognition systems use similar processing to extract specific target locations from audio/video data via a known feature vector for each target of interest.

A brute-force implementation of the approach described above includes high-sampling-rate acquisition of DCP signals and transmission of uncompressed DCP signals to an upstream location for comparison with multiple UCPs. This processing

clearly establishes an estimate for presence/absence of the downstream device (represented by its DCP) in the aggregated current profiles of several feeders (the UCPs). Unfortunately, high-rate acquisition and transmission of DCP data from multiple meters is not feasible using conventional AMR/AMI network infrastructure.

For example, assuming a 20kHz sampling rate at the meter with 16-bit resolution per-sample, the uncompressed bandwidth required for transmission of each DCP would exceed 320kbps. This data bandwidth can't be supported within existing remote metering infrastructure networks, particularly if thousands of meters were attempting to transmit usage data in addition to DCP profiles. As a result, to perform the described grid mapping operation using DCP data, some form of (lossy) compression of the DCP prior to transmission and processing at the upstream location is a critical notion. The compression or feature extraction operation on DCP data (which is subject to the upstream fidelity criteria) is implicit in the proposed system architecture because of limited data transmission bandwidth between downstream and upstream locations. The techniques for data compression, the fidelity criteria, and the upstream operations for estimation of device presence/absence, along with processing for geo-spatial and network-architecture indicators are the subjects of this paper and future work. Clearly, an operation which involved cross-correlation and time-coherence between a specific, uncompressed DCP and multiple UCPs is a valid approach to the problem. However, the compression methods or feature extraction methods which must be implemented at the downstream meters to preserve transmission bandwidth while simultaneously preserving recognizable features of the DCP are critical technologies.

The processing of the DCP prior to transmission is essentially a data compression or feature extraction operation. This operation must produce a set of features or compressed data which, when processed by upstream devices and compared with UCP data, produces clear indications of the presence or absence of a downstream device. The end-to-end system
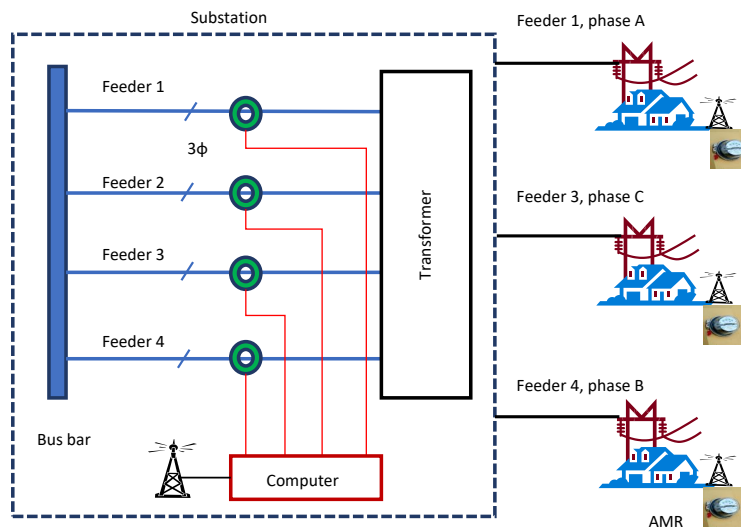
Fig. 6. Current attenuation in the distribution grid.

concept is very similar to feature extraction techniques which are used on fingerprint data. A reduced-fidelity representation of a fingerprint is captured, extracted, and stored. Then, the feature vector which uniquely identifies the fingerprint is compared to high-fidelity versions of a candidate fingerprint to create an indication of matching or similarity.

In the context of grid mapping and detection of current disturbances, techniques for DCP processing (or feature extraction) may include lossless data compression (e.g. LZW), transform coding (e.g. DCT/KLT), or other dimensionality reduction (e.g. ARMA, signal space techniques) followed by lossy compression, including scalar/vector quantization or signal space representations optimizing a weighted time-domain or frequency-domain fidelity criterion. This concept is important in allowing the upstream system to consume DCP data from all meters without exceeding system transmission capacity or interfering with bandwidth dedicated for AMR/AMI links. Thus, some feature extraction using raw sampled DCP data is necessary at the meter to reduce the size of the DCP data set to be transmitted.

However, these compression/extraction operations must retain important information in the signal for the mapping operation to succeed. Transport of the encoded, compressed, feature-extracted DCP data can be performed in-band using power line communications techniques which are intrinsic to grid infrastructure, or it can be performed out-of-band using communications infrastructure which is extrinsic to grid infrastructure. As a result, this technique does not require communication via the power line (from the meter to the substation). As such, no large amplifiers or coupling circuits are needed inside the smart meter itself. In fact most, if not all, of the required circuitry is already available inside a revenue-grade meter. In the simplest implementation, the DCP detected at the meter is sampled, processed for compression or feature extraction, and packaged for upstream transmission as part of the AMR/AMI meter data.

The DCP data from each meter can be aggregated at the utility central office or datacenter where the AMR/AMI data is received. In this fashion, computer hardware/software in the datacenter can analyze the UCP & DCP data and estimate each meter's grid location. The estimated grid location data is then stored in the utility's database updating their electrical grid map. A side benefit of this approach is that electrical mapping is done at a very slow rate. It only needs to happen once, and then periodic updates can happen much later. The DCP data can trickle out over the AMR/AMI wireless link for later analysis & registration using UCP information. Further, location errors due to DCP data snapshots can easily be corrected over time by keeping statistics on all computed locations and maximizing a likelihood function for meter or device location updates. In some cases, current disturbances detected at the meter and the substation feeder may be different, and the grid location computed/estimated for specific meters may be anomalous. However, errors in calculations will automatically be corrected as additional DCP & UCP data is collected and analyzed. Over time, an accurate grid location of each device will naturally emerge from the periodic mapping computations. This approach lends itself to a self-organizing network topology. Performing advanced system-level analysis such as power outage detection, power theft, power quality, or the like would require faster updates of the DCP data, and repeated comparisons with UCP data. In these cases, data compression or sub-sampled DCP data sets could mitigate any wireless capacity issue in a mesh network or other capacity-limited AMR/AMI system.

V. Concluding Remarks

We presented a novel method to accurately and intelligently map device locations in a smart grid. The novelty of this approach is the comparison of downstream current profiles (DCP) with the superposition of current profiles at the substation (UCP). Since small amounts of noise current

and perturbations will show up at the substation due to active devices on the grid, the electrical location of each meter can be determined by comparing passive line data from the meter location (DCP) against all the substation feeder lines (UCP).

Grid characteristics are constantly changing, producing multivariate non-stationary noise in the signal space of the grid. As a result, classic approaches involving channel models based on linear systems are futile and inefficient. Our method mitigates those issues by performing temporal comparisons of data at both points in the grid DCP and UCP. Feature extraction or compression of the sampled data at the meter or downstream location is important to reduce the size of the transmitted DCP. This allows the method to scale easily, given that it must service a large number of meters (and other devices) connected to each substation. GPS data from each smart meter is already available to assist in the reconciliation of geo-spatial location with electrical location.

We believe that the proposed technique will be a valuable addition to the grid. A patent based on the core idea of this paper was filed recently [8].

REFERENCES

[1] "Smart grid," https://energy.gov/oe/services/technology-development/smart-grid, accessed: 2015,2016.

[2] E. Khan, B. Adebisi, and B. Honary, "Location based security for smart grid applications," *Energy Procedia*, vol. 42, pp. 299–307, 2013.

[3] X. Fang, S. Misra, G. Xue, and D. Yang, "Smart grid - the new and improved power grid: A survey," in *IEEE Communications Surveys and Tutorials*, vol. 14, 2012, pp. 944–980.

[4] A. R. Sallam and O. P. Malik, *Electric Distribution Systems*. IEEE Computer Society, 2011.

[5] S. Kaplan, "Smart grid. electrical power transmission: Background and policy issues," in *The Capital.Net, Government Series*, 2009, pp. 1–42.

[6] "Suppression of interference in power and communications signals," US Patent 20160049988 A1, 2012.

[7] "AMR vs AMI," http://www.elp.com/articles/powergrid_international/print/volume-13/issue-10/features/amr-vs-ami.html, accessed: 2014,2015,2017.

[8] "Location mapping of grid devices using features of passively-observed current disturbances," US Patent WO2015120141 A1, 2015.

Using Smart Sensors to Monitor Concrete Infrastructure Assets for Useful Life Prediction Modelling

Peter J. Schemmel

Institute of Photonics and Quantum Sciences
School of Engineering and Physical Sciences
Heriot-Watt University
Edinburgh, Scotland EH14 4AS
email: P.Schemmel@hw.ac.uk

John J. Schemmel
Evan D. Humphries

Ingram School of Engineering
Texas State University
San Marcos, TX 78666 USA
email: john.schemmel@txstate.edu
email: ec1149@txstate.edu

Abstract—**Cities operating smart infrastructure systems will soon be ubiquitous. Transportation, health, education, water treatment, water resource, storm water management, and waste management systems will all be monitored and controlled remotely by computer programs and asset managers. Researchers continue to make advances in sensor technology, power supplies, communication networks, data storage, and data interpretation methodologies. First generation monitoring systems are currently being deployed and evaluated. However, use of these monitoring systems to develop predictive models for approximating the remaining useful life of an asset is not receiving the same level of attention. This paper will outline a method for using sensor systems to develop empirical lifetime prediction models for concrete structures. Two monitoring systems capable of accomplishing this goal, one well-established and the other in its infancy, are examined. Developing such a tool will provide asset managers with increased warning of impending structural issues such that more efficient and effective repairs can be implemented.**

Keywords-concrete; infrastructure; life prediction; sensor.

I. INTRODUCTION

In the coming years, cities across the world will begin to deploy smart sensor systems to monitor local infrastructure. City leaders will support such initiatives as a means to improve quality of life for its citizens though improved safety, functionality, environmental impact, and economic efficiency of its infrastructure. Monitoring of transportation networks, water and waste management systems, hospitals, and other public works using sensors is no longer a novel concept. However, even today, this process relies heavily upon visual inspections carried out sporadically over time, likely by different individuals. Such evaluations are unreliable, in part, due to variances in the knowledge and experience among inspectors. Deploying smart sensor systems across a city's infrastructure will allow asset managers to evaluate structures remotely, continuously, and consistently. Furthermore, the inclusion of intelligent software has the potential to redirect a significant portion of the monitoring burden away from required human involvement. If considered from a different perspective, these systems can also help city leaders assess when any one of its assets is approaching its useful life and

whether it makes sense from a safety and economic viewpoint to repair the structure.

Section II of this paper presents the components of a Technology Enhanced Infrastructure system. This section also introduces the premise that sensor data can be used to estimate the remaining useful life of an asset. The steps necessary for developing a useful life predictive model are then outlined in Section III. A simplified example illustrates the methodology involved in creating a predictive model. Section IV further explains the process of creating a model by examining the how a commercial sensor monitors concrete maturity in real time. An innovative means for monitoring stress in a concrete structure using radio waves is discussed next. This remote sensing device uses principles from physics, electrical engineering, and construction materials to measure stress in concrete. The paper concludes with a summary of the process for using sensor data to develop a predictive life model.

II. TECHNOLOGY ENHANCED INFRASTRUCTURE SYSTEMS

Technology Enhanced Infrastructure (TEI) systems have four elements in common: an array of physical assets, an inventory of embedded, attached and remote sensors, a data communication and storage network, and a cohort of asset managers. Before engineers and scientists can create an efficient, effective, and comprehensive TEI monitoring system for a city they must have a holistic understanding of the city's structural inventory, be aware of available sensor systems, and understand the informational needs of the asset management team. For example, the type of physical asset, its geographic location, its expected use, and relationship to other assets will all contribute to determining the relevant structural properties and performance data to be monitored. Communication networks, data storage, and power requirements will further define the specifications for a monitoring system. Intentions for quantifying, displaying, and interpreting the transmitted data must also be considered. Lastly, all this information, along with the objectives and goals of the asset managers, must pass through a sensor selection protocol.

Several research groups have begun the process of developing and deploying TEI systems to understand how future systems should be designed and implemented [1] - [4]. While this work is critically important, there is an unrealized

opportunity to exploit these systems for the betterment of a city and the general public. In addition to current applications, smart sensor technology can be used to inform asset managers of the remaining useful life of a structure and help them predict when and where failures might occur. Proposed herein is a methodology for developing an alternate use for a TEI system. In addition to monitoring a structure, TEI systems can be used to determine the remaining useful life of a structure. Two such systems for use with concrete structures, and capable of accomplishing the desired goal, are examined here. One system uses temperature sensors and maturity concepts to predict strength while the other, still in its infancy, uses radio frequencies to monitor stress.

III.   A METHODOLOGY FOR DEVELOPING EMPIRICAL LIFE PREDICTION MODELS

TEI networks capable of predicting the remaining useful life of a structure would be an invaluable resource for infrastructure asset managers. Having knowledge of an approximate time when major and minor repairs would be required for a structure would allow asset managers to schedule and budget these repairs in a more efficient and cost effective means. Being able to purchase repair materials in advance when prices might be lower, scheduling manpower to limit idle time, and mobilizing manpower in advance of a repair would ultimately improve the economic efficiency of a city's entire infrastructure inventory. For example, specific repairs might be explicitly scheduled on a recurring basis to extend the life of a structure. Alternatively, use of a structure by the public could be managed to prolong its life or maintain adequate safety, such as with load ratings for bridges. To realize these advantages requires an empirical lifetime prediction model based upon actual field data captured by a smart sensor and transmitted over a communication network.

Building a proposed life prediction model involves the following steps. First, one or more sensors must be selected that measure the desired structural parameters, recognizing that these parameters will vary as a function of the structure's age. For example, increases in stress and strain due to the corrosion of reinforcement bars in a concrete slab can lead to cracking and potential structural failure. In this instance the selection of a fiber Bragg grating strain sensor or electrical impedance sensor would be an appropriate selection. Alternatively, anemometers and vibrational measurements, which are often employed in early versions of TEI systems, are not well suited to predicting remaining life. This is because these devices primarily measure transient events. While such events are certainly significant as they can eventually lead to a structural failure, they do not vary with the age of the structure.

With a suitable sensor selected, the relationship between a measured property and a structure's age must be established. Clearly, this step is difficult to accomplish as waiting for full sized structural elements to fail is impractical. Therefore, correlations between measured properties and structural health must be established. One means for defining a correlation is through accelerated laboratory testing. As an example, sensor data can be recorded concurrently with the fatigue testing of metals subject to accelerated heat treatments.

Other examples involving concrete include freezing and thawing, alkali-silica, and sulfate attack behavior. Regardless of the material and parameter being evaluated, accelerated laboratory testing must continue to the defined failure of the material. While sensors may still need to be developed to measure some structural parameters in the field, accelerated laboratory tests for many materials are already available or well under development.

An example of an empirical model of measured sensor data as a function of a structures age is shown in Figure 1. This is the next step in establishing a predictive model. This chart plots the value of an expected measured parameter as a function of age. Regions above and below the measured data constitute an acceptable range for the parameter. An empirical model of this nature should be refined and adjusted over time as additional field data is recorded. However, as more monitoring systems are deployed and data is collected, it will be possible to establish an open source library of "standard parameter values."

The final step in predicting life expectancy is to use the library of standard parameter data to estimate the remaining life of a structure. In turn, this will provide asset managers with ample warning of the need for impending repairs. Two cases studies are presented below where work on life prediction models is being conducted.

IV.   CONCRETE STRENGTH PREDICTION USING RELATIVE HUMIDITY SENSORS

Maturity is a relatively simple concept associated with concrete where time, temperature, and relative humidity (RH) are used to estimate the early age in-place strength of concrete. This concept assumes that concrete mixtures with similar maturity indices, a computed value, will have similar strengths regardless of their individual age, temperature, or RH histories. The relationship between maturity index and in-place strength, as shown in Figure 2, is established from laboratory calibration testing for each individual concrete mixture. ASTM C1074 Standard Practice for Estimating Concrete Strength by the Maturity Method [5] defines the protocol for computing the maturity index. Today, several companies market sensors to monitor concrete age, temperature, and RH, though ASTM does not require RH be measured. When in-place, these sensors perform the necessary computations, based on prior laboratory calibration, to establish a measured maturity index. In general, that information is sent to a cellular phone where the maturity index is presented with a calibration curve and the associated concrete strength. An example of a modern sensor and smartphone display are provided in Figure 3 [6] and Figure 4 [7]. While not detecting a "failure" event, these sensors and the maturity concept can be used to create a predictive model. As opposed to considering the development of strength from zero to that associated with a particular maturity index, focus can instead be placed on the later portion of the index/strength curve. Again, refer to Figure 2. Rather than concentrating on the estimated concrete strength at any moment in time, attention can be given to the remaining strength capacity in the concrete. In other words, how much more strength is the concrete likely to develop within some period of time. This

information could have ramifications as to the time remaining until formwork can be removed or when vehicles might be allowed to travel across a pavement patch. Although basic in

nature, this is a very clear example of how sensor technology and laboratory data can be used to create a predictive model for concrete.
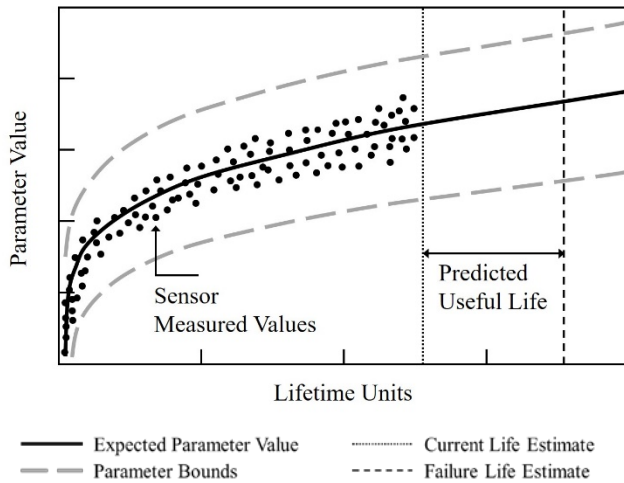
Figure 1. Simulated sensor data with depiction of predictive useful life.
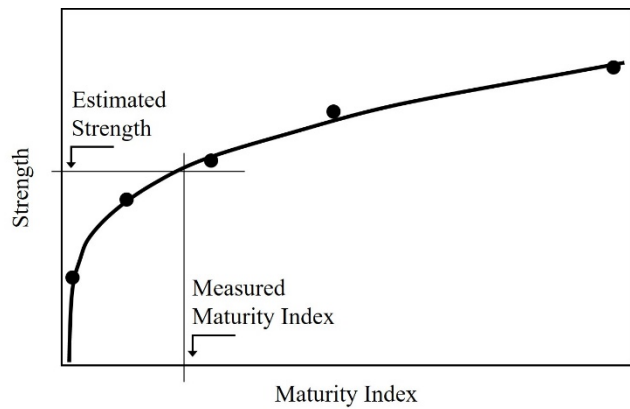
Figure 2. Graphic depiction of the maturity method.

Figure 3. Embedded sensor monitors temperature and relative humidity, calculates strength by ASTM C1074. (Courtesy of ConcreteSensors, http://www.concretesensors.com/products/).

Figure 4. Cellphone interface for embedded maturity sensor. (Courtesy of ConcreteSensors, http://www.concretesensors.com/)

V. CONCRETE STRESS MEASUREMENTS USING RADIO FREQUENCY

A research collaboration housed in the School of Engineering at Texas State University is employing principles from physics, electrical engineering, and construction materials to develop a novel approach for the measurement of stress in concrete. This approach employs radio frequency illumination to measure stress. In this study, properties of concrete specimens are measured remotely using lensed horn antennas connected to a vector network analyzer. The parameters being measured are related to concrete strength and are known to be correlated to the age of concrete. Currently, testing is being conducted to establish an empirical lifetime prediction model with appropriate boundaries on the measured parameters. Calibrating field measurements are planned for the near future. Correlation of the field and laboratory data will then be used to refine the predictive model. Once the predictive model has been validated, research

will examine the sensitivity of the model to variations in the concrete's constituent materials and proportions.

VI. CONCLUSION AND FUTURE WORK

This paper outlined a method for using TEI systems to develop a predictive model for estimating the remaining life of a structure. Not only will this contribute to more resilient structures it will also extend the functionality and economic feasibility of a monitoring system. While TEI systems will soon become common place, utilizing them to predict the need for major structural repairs is still a novel concept. However, efforts are underway to develop an empirical lifetime prediction model for concrete structures using field data measured and transmitted via a TEI system.

Developing a predictive model is a multi-step process that relies on engineering parameters being measured in the field by smart sensors. The measured parameters must be a function of, and vary with, the age of the structure. Field data is then correlated with comparable laboratory garnered from

accelerated testing of the construction material. These two data sets establish the foundation for the predictive model. Over time, an open source library of engineering parameter values with accepted bounds will be populated and routinely updated for use by the engineering community.

Two sensor monitoring systems that can be used to create predictive models were reviewed. One sensor system is based on well-established principles while the other has brought several science and engineering disciplines together to create a novel solution.

The overarching objective of the concept proposed here is to provide asset managers with a new tool which they can use for early warning of impending structural issues, including failure. Such a tool would allow for more efficient and effective repairs to an infrastructure asset with the goal of maintaining, or improving, its safety and value. While this paper has focused on concrete structures and parameters, it is envisioned that this approach can be applied to any infrastructure asset built from a construction material with a time variable behavior.

REFERENCES

[1] N. A. Hoult, P. R. A. Fidler, P. G. Hill, and C. R. Middleton, "Long-term wireless structural health monitoring of the Ferriby Road Bridge," J. Bridge Eng., no. 15, pp. 153-159, 2010.

[2] N. A. Hoult, P. R. A. Fidler, P. G. Hill, and C. R. Middleton, "Wireless structural health monitoring at the Humber Bridge UK," Proc. ICE-Bridge Eng., vol. 161, no. 4, pp. 189-195, 2008.

[3] S. Jang et al., "Structural Health Monitoring of a cable-stayed bridge using smart sensor technology: deployment and evaluation," Smart Structures and Systems, vol. 6, no. 5-6, pp. 439-459, 2010.

[4] S. Cho et al., "Structural Health Monitoring of a cable-stayed bridge using smart sensor technology: data analysis," Smart Structures and Systems, vol. 6, no. 5-6, pp. 461-480, 2010.

[5] ASTM C1074-11 Standard Practice for Estimating Concrete Strength by the Maturity Method, ASTM International, West Conshohocken, PA, 2011, www.astm.org.

[6] Structural Health Systems, Inc. Embedded sensor, digital image, Structural Health Systems, Inc., provided 9 March 2017, via electronic mail.

[7] Structural Health Systems, Inc. Cell phone interface screenshot, digital image, Structural Health Systems, Inc., provided 9 March 2017, via electronic mail.